Geochemistry and 14C dating of guano deposits in the Karaftu Cave, Kurdistan, Iran: Implication for palaeoenvironment

Hadi Amin-Rasouli (h.aminrasouli@uok.ac.ir)
University of Kurdistan
Masayo Minami
Nagoya University
John Armstrong-Altin
National Autonomous University of Mexico
Nasim Haghighat Jou
University of Kurdistan
Mehdi Moradi
Geological Survey of Iran

Research Article

Keywords: Karaftu Cave, Guano, REEs, Secondary minerals, Environment, 14C dating

Posted Date: April 27th, 2023

DOI: https://doi.org/10.21203/rs.3.rs-2811114/v1

Version of Record: A version of this preprint was published at Environmental Monitoring and Assessment on September 5th, 2023. See the published version at https://doi.org/10.1007/s10661-023-11624-9.

Abstract

Karaftu Cave in the northwest of Divandareh includes four floors plus an underground area. The bat hall and its underground area are covered with guano deposits. ^{14}C dating indicates the onset of guano deposition is about 14260±50 BP years, and its average accumulation rate is about 4.1 mm/yr for depths of 360 to 205 cm. Bacterial and fungal metabolisms decay guano, release acids, and disperse large amounts of microorganisms inside the cave. Interactions between acids and guano caused leaching, dissolution, change in the distribution, and abundance of elements, which leads to the formation of secondary minerals in guano. These variations in minerals and elements also depend on the local climatic conditions. Distribution of elements in the Ce/Ce* verse Pr/Pr* diagram and the correlation coefficient between Ce and Mn display three different paleoclimate conditions (dry, wet, and dry) during the accumulation of the guano. Also, dolomite, phosphate, and iron oxide minerals have been formed during the passage of water through bedrock beneath the guano. This water is unsuitable for drinking and harmful to the organisms in the region. Effect of these acids on the substrate also leads to the collapse of the cave floor, generation of a new underground, fall in the groundwater level, change in the groundwater drainage system, drying of springs around the cave, loss of green cover, and a negative impact on the ecosystem in the region. To keep the cave environment clean and remove these problems, it is better to harvest guano and use it as fertilizer.

1. Introduction

Caves are natural underground cavities that begin to form very slowly due to the dissolution of carbonate rocks by groundwater. First, they occur under the water table and become dry as the water table drops from the cave bottom. They serve as roost sites for bats in the dark zone.

Cave deposits are divided into chemical, biochemical, and terrigenous categories (Wurster et al., 2015; Dimkić et al., 2020). One of the biochemical cave deposits is bat guano, the fecal material of bats and birds (e.g., Onac and Vereş, 2003; Cleary et al., 2019; Sakoui et al., 2020). The accumulation of bat guano often requires considerable time, during which various geochemical processes, such as weathering, leaching, and changes in environmental conditions, occur. These processes affect the distribution of secondary minerals, trace elements, REEs, and their proportions (e.g., Brauer et al., 1999; Smol and Cumming, 2000).

Bat guano deposits are a significant continental paleoenvironmental archive of climate change for semi-arid and tropical regions (e.g., Wurster et al., 2010). Some researchers have studied ^{14}C, stable isotopes, palynology, secondary minerals, and elemental variations in guano deposits to determine paleoenvironment and age (e.g., Johnston et al., 2010; Batina and Reese, 2011; Onac et al., 2014; Forray et al., 2015; Wurster et al., 2017; Cleary et al., 2018, 2019; Onac, 2019; Audra et al., 2021; Cleary and Onac, 2021; Tsalickis et al., 2021).

Karaftu Cave is located 67 km northwest of Divandareh (46˚ 52' 30" E and 36˚ 20' 02" N), Kurdistan province. According to the climatic divisions of De Martin, the region has a semi-arid climate with mean annual precipitation of 395 mm. The mean temperature of the area is 13.9 ˚C/yr, with a minimum of − 9/8 ˚C in February and a maximum of 31/4 ˚C in July.

The cave entrance is located at 2030 m above sea level and 25 m from the surrounding area. It is about 800 m long, with chambers and corridors at four levels and an underground hole at the bat hall on the second floor. The bedrock of the bat hall is covered by bat guano with an average of 2 m in thickness over a surface of several square meters (Fig. 1A- G) (Haghighat jou, 2017; Amin-Rasouli et al., 2021). The bat species are *Rhinolophus ferrumequinum* (Schreber, 1774), *Rhinolophus mehelyi* (Matschie, 1901), *Myotis blythii*, and *Miniopterus pallidus* (in Benda et al., 2012). These species feed on terrestrial arthropods, moths, and insects and produce phosphorus guano (Wurster et al., 2010).

2. Geological setting and stratigraphy

Karaftu Cave is located in the northern Sanandaj-Sirjan Zone (SaSZ), west Iran (Stöcklin, 1968). The SaSZ originated from the subduction of the Tethyan oceanic lithosphere under the southwestern border of Central Iran, leading to intermediate to felsic plutonic and volcanic activity from the Jurassic to Quaternary within and adjacent to the SaSZ (Mohajjel et al., 2003) (Fig. 2A). It is 800 km long and 150–250 km wide, situated between the Zagros fold-thrust belt in the southwest and Urumieh- Dokhtar magmatic arc in the northeast (Stöcklin and Nabavi, 1972).

The cave formed in the f-member of the Oligo-Miocene Qom Formation (Fig. 2A, B). The Qom Formation includes nine lithostratigraphic members (a- to f- members: a-member = basal limestones, b- member = sandy marls, c1- member = limestones, c2- member = evaporates, c3- member = limestones, c4- member = pelagic marls, d-member = evaporates, e-member = green marls, f- member = top limestones contain coral reef, red algae, porcelaneous and large hyaline foraminifera, bryozoan, echinoderms, and gastropods) in the type locality near the town of Qom (Bozorgnia, 1965; Reuter et al., 2009).

The studied guano is situated in the bat hall with no dripping water and active stream, but water has accumulated in several small areas. The bat hall's temperature and relative humidity average are 16 ˚C and 35%, respectively. This study aims to determine the distribution of chemical elements, secondary minerals, the accumulation rate of guano, age, paleo-redox conditions, biogenic activities, and climate changes during the accumulation of guano in the Karaftu Cave. In addition, the influence of solution leaching from guano to the groundwater, their environmental hazards, and organisms in the guano deposits are also discussed in this study.

3. Methods

Nineteen samples were collected vertically depending on the variations in color (approximately 50 g) from the base to the top of the guano deposits in the Karaftu Cave. They were mainly brown colored, moist, and exhibited subtle stratification except at depths of 250 and 165 cm, in which the samples are dark red-brown and white, respectively. Samples were kept at − 16 ˚C in the laboratory until analyzed. For analyses of trace elements and rare earth elements (REEs), ~ 70 mg of each sample was decomposed with 3 mL of HF (38%) and 0.5–1 mL of $HClO_4$ (70%) in a covered polytetrafluoroethylene (PTFE) beaker at

120–140 °C. The dissolved samples were dried at 140–160 °C on the hot plate with infrared lamps. The samples were dissolved in 10 mL of 2–6 M HCl, and then resulting solutions were used for trace elements (plus REEs) analysis. Trace element compositions were determined by inductively coupled plasma–mass spectrometry (ICP–MS), Agilent 7700x, at the Geological Survey of Iran. The detection limits for elements are between 0.08 and 0.6 ppm.

The secondary minerals were recognized herein based on scanning electron microscopy- energy dispersive X-ray spectrometry (SEM-EDX), except carbonate minerals, which were performed on samples at the University of Kurdistan. Also, five thin sections from the bedrock of guano deposits were prepared and petrographically investigated under the polarized microscope at the University of Kurdistan.

Samples for radiocarbon dating were selected at depths of 205 cm and 360 cm. Their organic acids and secondary carbonate were removed and digested separately in 2 M HCl at 80 ˚C for 8 hours. The samples were washed twice with distilled water until the solutions were clear and soaked in 1 M KOH solution at 80˚C for 2 hours. Samples were digested with 1 M HCl for 2 hours to remove extra KOH. Afterwards, they were dried at 140 ˚C and burned in a quartz tube to produce CO_2. The purified CO_2 was reduced to graphite with an iron catalyst and hydrogen at 650˚C for 6 hours. ^{14}C dating was performed by accelerator mass spectrometry (Model 4130-AMS, High Voltage Engineering Europe) at the Center for Chronological Research (CCR), Nagoya University, and calibrated using the IntCal13 curve (Reimer et al., 2013).

4. Results and discussion

4.1 ^{14}C dating

Radiocarbon dating is a technique for determining the age of an object containing organic matter. Two samples were collected from the depth of 360 cm and 205 cm to determine the beginning and rate of Karaftu guano accumulation based on ^{14}C dating. The Carbon-14 dating of guano deposits from these depths provides ages 14260 ± 50 years BP and 13845 ± 50 years BP, respectively (Table 1). That indicates the start of guano deposition, from a depth of 360 cm, was after the Last Glacial Maximum, LGM (Street-Perrott and Perrott, 1990). During this time, the climate was similar in most areas (Fig. 3), and its evidence has been recorded around the world and near the study area in Zaribar Lake, northwest of Kurdistan (van Zeist and Wright, 1963; van Zeist and Bottema, 1977). Based on the ^{14}C dating from the depths of 360 and 205 cm, and the difference between compacted (1.85 gr/cm^3) and non-compacted (1.7 gr/cm^3) guano densities, the average deposition rate for these depths was about 4.1 mm/year.

4.2. Trace elements

Trace-element abundances in sediments and sedimentary rocks allow us to reconstruct paleodepositional conditions (e.g., Riquier et al., 2006; Tribovillard et al., 2006; Armstrong-Altrin et al., 2021, 2022). They are released into the environment from the natural weathering of rocks and various sources related to human activity. The concentration of these elements may directly or indirectly affect the chemical composition of foodstuff and animal feed (e.g., Haluschak et al., 1998). Climatic/chemical weathering degree is one of the factors (e.g., Gangloff et al., 2016) which controls the transfer of trace element ions from the soil into plants and then into animals plus their feces/herein bat guano. Concentrations of trace elements in plants are often positively correlated with the abundance of these elements in soils and underlying rocks (Kabata-Pendias, 2010) plus wet climate (e.g., Cucurić et al., 2011; Dodge-Wan et al., 2017). As a result, trace elements in guano deposits are considered as a tool to determine source rocks and environmental changes.

In the study area, the guano profile indicates fluctuation in the distribution of trace elements from the top to bottom (Table 1). Based on the sharp change in their distribution, they show at least three units/cycles with 2–3 smaller cycles in each (Fig. 4). Fluctuations in trace elements mainly depend on weathering and local mineral resources in the profile. The mean value of elements in unit 2 is higher than in units 1 and 3 (Table 2), indicating that they formed under wet/rainy conditions (Cucurić et al., 2011; Dodge-Wan et al., 2017).

The geochemical data show variation in the abundance of Zr and Ti, same as other trace elements, except at the bottom. These elements are primarily immobile after deposition, and their amounts record the accumulation rate of guano deposits, with high abundance indicating a low guano accumulation rate and vice versa. So, the high Zr and Ti values at their bases represent the lack of guano deposits (e.g., Taylor and McLennan, 1985; Bird et al., 2007).

4.3. REEs

REEs are a group of elements, from lanthanum to lutetium, with similar physicochemical properties, because of their specific electronic configurations (except Ce and Eu, which exhibit multiple valences). REEs are divided into two light REEs (LREEs) from La to Eu and high REEs (HREEs) from Gd to Lu (e.g., Kato et al., 2011). Because of the systematic variation in their behaviors, REEs have received considerable attention in the geoscience field. For instance, REEs have been used to explain geochemical processes, including weathering and palaeoenvironmental changes (Armstrong-Altrin 2020). Geochemical data indicate two sharp fluctuations in the amounts of REEs at depths of 270 cm and 140 cm. Fluctuations in the concentrations of these elements represent similar trends throughout the depth of the profile. According to them, three climatic (dry, wet, and dry) conditions are distinguished through the guano profile, the same as the distribution of trace elements (Fig. 5).

Table 1

ICP-MS analysis and ^{14}C dating of the guano samples.

Depth of sample	0(top)	10	30	50	70	90	120	140	165	185	205	240	255	260	270	290	310
Trace elements (ppm)																	
Ti	1166	935	986	903	835	909	593	1747	1317	1078	1312	1482	809	742	968	1020	784
Mn	159	171	118	102	77	124	130	288	242	84.9	158	211	119	63.7	96.0	221	145
Mo	7.94	6.82	7.87	11.9	17	19.6	10.0	29.7	28.2	21.0	25.2	46.0	11.6	3.82	4.72	18.9	14.3
Ba	157	109	163	132	121	222.9	106	339	309	175	352	384	164	101	185	241	210
Rb	28.3	21.9	14.5	21.3	21	23.2	14.1	34.9	34.9	19.1	17.4	29.4	15.9	20.5	20.0	22.0	20
Sr	70.1	66.3	70.7	49.3	35	63.4	54.0	61.2	77.0	40.3	34.2	39.0	32.0	48.6	59.3	52.5	47.0
Y	14.9	10.9	13.4	8.90	8.73	11.9	4.49	15.3	19.7	8.08	16.7	18.7	8.85	3.76	3.87	5.84	3.8
Zn	313	271	560	466	622	750.0	316	1250	1002	606	1010	1613	666	247	546	892	838
Cu	299	277	287	1334	1007	2035	832	4329	3812	1174	2510	5231	1602	443	786	1547	928
Ni	11.4	15.1	9.93	28.0	26	45.7	41.1	57.5	47.4	36.4	51.9	93.4	25.0	11.1	15.1	26.7	18.3
Pb	11.5	9.12	11.9	9.90	7.91	12.7	6.20	19.3	12.7	9.18	12.8	29.5	9.65	5.05	7.12	11.1	0.0
Co	2.70	3.61	3.73	7.61	6.51	9.6	5.07	14.2	14.8	7.45	10.8	15.3	5.84	3.40	4.62	9.43	8.81
Sc	3.98	2.95	3.93	1.81	1.96	2.6	1.73	4.97	5.27	2.45	2.42	3.26	2.31	2.59	3.41	3.16	2.34
Zr	34.8	16.0	18.0	15.6	40.5	57.7	8.52	54.3	30.3	20.0	30.8	43.3	25.4	22.2	30.3	28.8	16.1
Th	2.16	1.53	2.16	1.30	2.06	1.15	0.88	3.29	3.88	1.29	1.65	2.23	1.56	1.64	1.89	1.66	1.00
U	1.96	1.41	1.60	1.30	1.40	1.49	0.82	2.91	2.45	1.53	2.25	3.75	1.21	0.58	0.61	0.87	0.57
Nb	4.51	3.02	3.61	2.69	4.51	5.5	1.92	9.83	5.64	5.17	5.17	9.55	5.41	4.51	5.07	5.88	5.36
Hf	0.62	0.40	0.50	0.35	0.43	0.61	0.33	1.21	0.88	0.55	0.91	1.22	0.55	0.45	0.58	0.84	0.56
Ta	0.59	0.33	0.47	0.32	0.43	0.46	0.26	0.63	0.76	0.35	0.42	0.85	0.53	0.32	0.49	0.73	0.75
W	1.77	1.53	2.17	2.68	3.68	2.36	2.50	6.28	7.28	3.20	3.54	5.57	2.61	1.04	1.34	2.46	1.7
REEs (ppm)																	
La	8.87	6.98	9.13	5.99	7.49	9.55	4.88	14.7	18.5	7.93	12.7	17.5	6.00	5.28	8.37	8.38	5.98
Ce	15.3	10.4	14.0	8.8	11.8	16.8	4.31	21.1	31.8	11.4	19.8	27.7	10.9	11.1	15.4	13.1	8.48
Pr	2.41	1.83	2.83	1.35	1.63	2.3	1.01	3.27	3.48	1.31	1.87	2.54	1.57	1.31	1.65	1.40	1.10
Nd	8.69	5.83	7.52	4.56	6.33	8.94	2.39	11.1	16.1	6.42	12.1	16.7	5.44	5.66	8.81	6.01	4.41
Sm	2.10	1.58	1.95	1.26	1.65	1.02	0.77	3.39	3.92	0.93	1.75	2.02	1.81	0.78	1.15	1.44	0.69
Eu	0.41	0.31	0.56	0.25	0.2	0.4	0.17	0.66	0.70	0.31	0.42	0.48	0.24	0.15	0.23	0.26	0.23
Gd	1.81	1.46	1.91	1.10	1.1	1.6	0.74	1.78	2.5	1.15	1.97	3.7	1.50	0.79	0.93	1.14	0.71
Tb	0.26	0.20	0.29	0.15	0.2	0.2	0.11	0.36	0.44	0.21	0.27	0.35	0.26	0.14	0.16	0.17	0.12
Dy	1.94	1.44	1.60	1.23	1.41	1.44	0.62	2.22	2.90	1.29	2.51	3.30	1.97	0.63	0.79	1.31	0.81
Ho	0.46	0.33	0.47	0.29	0.3	0.4	0.15	0.44	0.58	0.25	0.40	0.50	0.32	0.14	0.15	0.21	0.16
Er	1.03	0.72	0.83	0.66	0.7	0.8	0.42	1.50	2.14	0.56	1.20	1.44	1.11	0.39	0.48	0.81	0.37
Tm	0.21	0.15	0.19	0.12	0.1	0.2	0.07	0.28	0.33	0.10	0.15	0.18	0.14	0.07	0.09	0.09	0.07
Yb	1.10	0.66	0.81	0.64	0.76	0.79	0.38	1.17	1.61	0.75	1.30	1.58	0.81	0.35	0.39	0.58	0.45
Lu	0.20	0.13	0.14	0.11	0.10	0.14	0.07	0.25	0.27	0.09	0.23	0.29	0.15	0.07	0.09	0.14	0.07
∑LREE	37.8	26.9	36.0	22.2	29.0	39.1	13.5	54.2	74.5	28.3	48.7	66.9	36.3	24.3	25.3	30.6	20.9
∑HREE	7.01	5.08	6.24	4.30	4.57	5.61	2.55	8.02	10.75	4.39	8.04	11.34	6.26	2.57	3.07	4.44	2.75
∑REE	44.8	32.0	42.2	26.5	33.5	44.7	16.1	62.2	85.3	32.7	56.7	78.2	42.5	26.9	28.4	35.0	23.6

Depth of sample	0(top)	10	30	50	70	90	120	140	165	185	205	240	255	260	270	290	310
L/H $(Nd/Er)_{CN}$	2.63	2.53	2.85	2.15	2.78	3.47	1.80	2.31	2.36	3.59	3.16	3.61	2.48	4.60	3.56	2.32	3.77
Ratios																	
Ba/Sr	2.24	1.65	2.31	2.67	3.49	3.52	1.96	5.55	4.01	4.33	10.29	9.86	5.12	2.08	3.12	4.59	4.46
La/Sc	2.23	2.37	2.32	3.31	3.82	3.67	2.82	2.95	3.51	3.24	5.25	5.38	3.62	2.04	1.76	2.65	2.56
La/Th	4.10	4.57	4.24	4.61	3.64	8.31	5.56	4.46	4.76	6.12	7.70	7.86	5.36	3.22	3.17	5.03	5.99
La/Yb	8.0	10.6	11.3	9.4	9.9	12.1	12.7	12.5	11.5	10.6	9.8	11.1	10.3	15.1	15.5	14.5	13.3
Sc/Ni	0.35	0.20	0.40	0.06	0.08	0.06	0.04	0.09	0.11	0.07	0.05	0.03	0.09	0.23	0.23	0.12	0.13
Rb/Sr	0.40	0.33	0.21	0.43	0.61	0.37	0.26	0.57	0.45	0.47	0.51	0.75	0.50	0.42	0.34	0.42	0.43
Th/Co	0.80	0.42	0.58	0.17	0.32	0.12	0.17	0.23	0.26	0.17	0.15	0.15	0.27	0.48	0.41	0.18	0.11
Th/Sc	3.98	2.95	3.93	1.81	1.96	2.60	1.73	4.97	5.27	2.45	2.42	3.26	2.31	2.59	3.41	3.16	2.34
Th/U	1.11	1.09	1.34	1.00	1.47	0.77	1.07	1.13	1.59	0.85	0.73	0.60	1.30	2.81	3.09	1.91	1.75
Y/Ho	32.6	33.0	28.8	30.6	34.9	30.4	30.2	34.6	34.2	32.8	41.8	37.3	27.4	27.2	25.1	27.9	24.2
Ce/Ce^*_{SN}	0.76	0.67	0.63	0.72	0.78	0.82	0.45	0.70	0.91	0.80	0.91	0.93	0.90	0.89	0.95	0.87	0.76
Eu/Eu^*_{SN}	1.00	0.97	1.36	1.01	0.88	1.43	1.07	1.23	1.05	1.40	1.04	0.77	0.69	0.90	1.06	0.97	1.54
Pr/Pr^*_{SN}	1.22	1.37	1.61	1.25	1.10	1.12	1.83	1.25	0.90	0.89	0.70	0.69	1.00	1.16	0.82	0.93	1.05
^{14}C dating											13845 ± 50 BP						

$[Ce/Ce^*=2Ce/(La + Pr)]_{SN}$; $[Eu/Eu^*=2*Eu/(Sm + Gd)]_{SN}$; $[Pr/Pr^*=2Pr/(Ce + Nd)]_{SN}$; SN = Post Archean Australian Shale normalized; CN = Chondrite normalized (1989)

Table 2
Average of trace elements (TEs) and REEs for three units in the guano profile.

Depth (cm)	TEs	LREEs	HREEs	∑REEs	$(Nd/Er)_{CN}$
0-140	162.0	32.3	5.4	37.8	2.6
165–270	228.7	43.5	8.6	50.1	3.2
290–360	151.1	28.4	4.5	32.9	3.1

4.4. Paleo-redox conditions

Cerium and Eu anomalies usually occur in the natural environment and are applied to identify paleo-redox conditions (e.g., Albarede, 2011; Tostevin et al., 2016; Armstrong-Altrin and Machain-Castillo, 2016; Ramos-Vázquez et al., 2018, 2022). The REEs are typically in the 3 + oxidation state, but Eu occurs in divalent in strongly reducing environments. Europium anomalycan be calculated by comparing it with its neighboring REEs (Obaje et al., 2015):

$Eu/Eu^*_{SN} = 2Eu_{SN}/(Sm_{SN} + Gd_{SN})$ (Wherein SN refers to shale- normalized)

The Eu/Eu^*_{SN} (= 0.69 to 1.54) values of the samples show positive (Eu/Eu* >1) and negative (Eu/Eu* <1) anomalies, reflecting a change in conditions from reducing to oxidizing and vice versa during deposition. In Fig. 5, all patterns are similar except Eu/Eu^*_{SN}, which is sensitive to temperature changes, such as a thermometer, during the water-rock interaction (Nakada et al., 2017).

Cerium is the only lanthanide that undergoes oxidation from a more soluble 3 + to a less soluble 4 + valence state in low-temperature aqueous environments. Since $Ce^{4+}$is adsorbed more strongly than the other trivalent REEs, it is widely used as an indicator of paleoredox conditions (Sanematsu et al., 2013; Ling et al., 2015). Oxidation and reduction conditions generally form positive and negative Ce anomalies, respectively (e.g., Alibo and Nozaki, 1999). Ce anomaly is calculated from the following equation (Obaje et al., 2015):

$Ce/Ce^*_{SN} = 2Ce_{SN}/(La_{SN}+Pr_{SN})$

Samples show the Ce/Ce^*_{SN} values from 0.45 to 0.95. Bau and Dulski (1996) proposed the Ce/Ce*-Pr/Pr* diagram to recognize the true Ce anomalies (Fig. 6A). Studied samples fall in the IV, IIa (from 255 cm depth), and IIIb fields in this diagram and show three climatic conditions (Table 3).

Table 3. The table shows the locations, descriptions of the samples in the Ce/Ce*-Pr/Pr* diagram and the changes in climatic conditions along the studied profile.

Depth (cm)	Values		Ce anomaly based on Ce/Ce* vs. Pr/Pr* diagram (after Bau and Dulski, 1996)		
	Ce/Ce^*_{SN}	Pr/Pr^*_{SN}	Field	Description	
0	0.76	1.22	IIIb	real negative Ce anomaly	
10	0.67	1.37	IIIb	real negative Ce anomaly	
30	0.63	1.61	IIIb	real negative Ce anomaly	
50	0.72	1.25	IIIb	real negative Ce anomaly	Dry
70	0.78	1.10	IIIb	real negative Ce anomaly	
90	0.82	1.12	IIIb	real negative Ce anomaly	
120	0.45	1.83	IIIb	real negative Ce anomaly	
140	0.70	1.25	IIIb	real negative Ce anomaly	
165	0.91	0.90	IV	positive La-anomaly disguises positive Ce anomaly	
185	0.80	0.89	IV	positive La-anomaly disguises positive Ce anomaly	
205	0.91	0.70	IV	positive La-anomaly disguises positive Ce anomaly	
240	0.93	0.69	IV	positive La-anomaly disguises positive Ce anomaly	Wet
255	0.90	1.00	IIa	positive La-anomaly causes apparent negative Ce-anomaly	
260	0.89	1.16	IV	positive La-anomaly disguises positive Ce anomaly	
270	0.95	0.82	IV	positive La-anomaly disguises positive Ce anomaly	
290	0.87	0.93	IIIb	real negative Ce anomaly	
310	0.76	1.05	IIIb	real negative Ce anomaly	Dry
350	0.81	1.23	IIIb	real negative Ce anomaly	
360	0.61	1.43	IIIb	real negative Ce anomaly	

Manganese is one of the significant carrier phases for excess Ce (De Baar et al., 1988; Sholkovitz et al., 1994; De Carlo et al., 1997; Bau, 1999; Ohta and Kawabe, 2001; De Carlo and Green, 2002) and the reduction/dry and oxidation/wet conditions are determined based on the low and high Ce- Mn correlation coefficient, respectively. They have the weak correlation coefficients in depths of 360– 290 cm (R^2 = 0.35) plus 140 – 0 cm (R^2 = 0.36), and very high ones in the 270– 165 cm (R^2 = 0.98) depths (Fig. 6B- D). These indicate that drastic changes in sedimentary conditions occurred between depths of 140–165 cm and 270–290 cm. Therefore, from its base towards the top, the studied guano has been deposited under dry (depth of 360 – 290 cm), wet (depth of 270 – 165 cm), and dry (depth of 140 – 0 cm) conditions (Table 2).

4.5. Secondary minerals

Bat guano deposits are sites of various complex reactions (mainly biologically driven), ultimately releasing organic, nitric, carbonic, phosphoric, and sulfuric acids (Forti, 2001). The acids then interact with the carbonate bedrock or cave sediments, cause leaching and dissolution, and form unique authigenic minerals (Bridge, 1973; Karkanas et al., 2002; Shahack-Gross et al., 2004) within the cave deposits. These minerals are complex, and their distributions provide critical information concerning the weathering processes that originated the hosting cavities (e.g., Onac and Vereş, 2003; Plan et al., 2012).

Karaftu Cave includes carbonate, sulfate, phosphate, and nitro minerals. Carbonate minerals are the most abundant chemical/biochemical minerals (Cañaveras et al., 2001; Cuezva et al., 2009) (Fig. 7A- C).

Sulfate minerals in the Karaftu Cave consist of gypsum and cesanite (Fig. 8A- E). Gypsum presents along with phosphate minerals in the entire studied profile. Bacterial and fungal metabolisms decay guano and release H_2S acid. Hydrogen sulfide constitutes an abundant source of chemical energy (i.e., food) for certain bacteria. They eat hydrogen sulfide, breathe oxygen, and produce sulfuric acid as metabolic waste (e.g., Wells et al., 2022). Interaction of guano-derived sulfuric acid with carbonate particles leads to Ca-sulfate deposition (e.g., Onac et al., 2009; Giurgiu and Tamas, 2013). The general reaction is:

$$CaCO_3 + H^+ + SO_4^{2-} + 2H_2O \longrightarrow CaSO_4.2H_2O + HCO_3^-$$

That is the source of gypsum within cave deposits (Hill and Forti, 1997), and it is not alone as a good indicator for identifying cave conditions (e.g., Onac et al., 2002).

The most numerous biogenic minerals, in terms of anion types, are phosphates, after oxides, and carbonates (e.g., Tazaki, 2006). The precipitation of phosphate minerals in caves is related to PO_4^{3-} leaching from the guano and combining with the Ca^{2+}, Fe^{2+}, Al^{3+}, K^+, Na^+, and Mg^{2+} ions (Onac and Veres, 2003). Phosphate minerals are taranakite, brushite, whitlockite, francoanellite, leucophosphite, spheniscidite, phosphammite, and pyrocoproite in the guano deposits of Karaftu Cave (Figs. 9A- I, and 10A- F).

A comparison between the distribution of secondary minerals and Ce/Ce*, in the studied profile, indicates that taranakite forms in wet conditions. However, whitlockite, urea, and cesanite only occur in dry ones (e.g., Bridge, 1973; Onac and Vereş, 2003; Forti et al., 2004; Snow et al., 2014; Audra et al., 2021). Therefore, they can be climate indicator minerals, but other minerals (because of their presence in both conditions) cannot be so (Table 4). These variations in minerals and elements are also mainly related to the local paleoenvironmental and climatic conditions (Tsalickis et al., 2021).

Karaftu Cave consists of urea ($CO(NH_2)_2$) and niter (KNO_3) minerals (Fig. 11A- C). These minerals are highly soluble and precipitate only under warm and dry conditions or during guano combustion due to an exothermic reaction of guano decay (Onac and Forti, 2011; Audra et al., 2017; Audra et al., 2021).

Table 4. The distribution of secondary minerals through guano deposits and their comparison with climatic conditions resulting from the Ce/Ce^*_{SN} -$Pr-Pr^*_{SN}$ diagram.

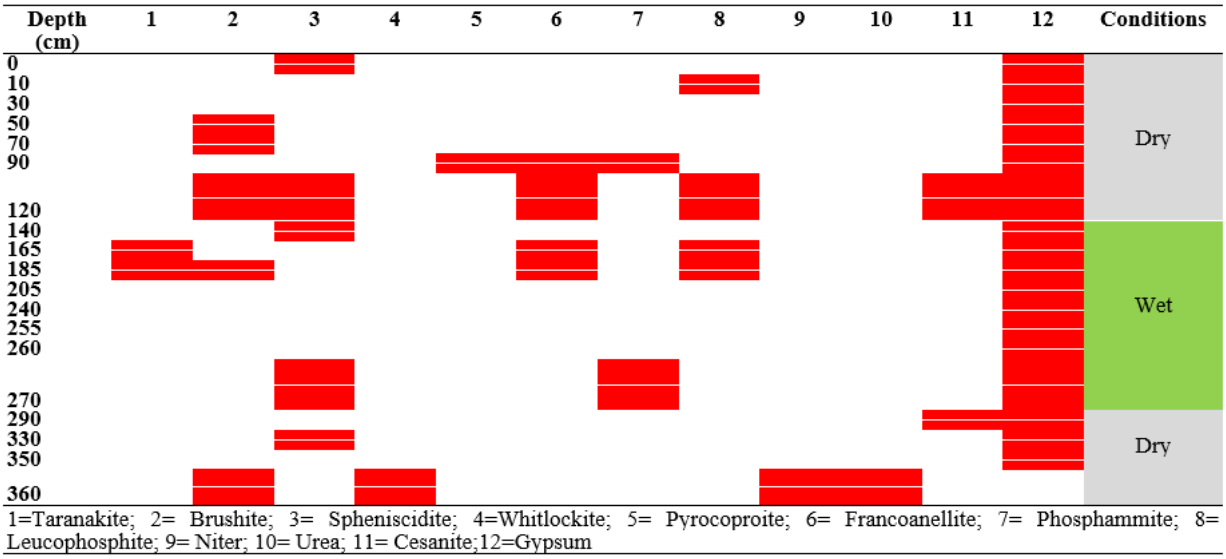

The interaction between acidic solutions derived from guano and carbonate bedrock has resulted in the deposition of dolomite, phosphate, and iron oxide minerals in the bedrock. The solution pH may be very low because the high chemical stable echinoderm fragments have been changed to dolomite (Fig. 12A-B).

4.6. Biogenic activities

Caves are minimally affected by environmental conditions and are used as permanent residences by bat colonies. All kinds of life forms (i.e., viruses, bacteria, fungi, protists, plants, and animals) are common in caves (Romero, 2009; Culver and Pipan, 2019), both active or fossilized states, and a range of different types of habitats (i.e., rocks, springs, pools, cave walls, or even dispersed in the air). SEM photomicrographs of guano samples show various microorganisms (Fig. 13A- E). They most probably contribute to the formation of secondary minerals and the cycling of organic and inorganic nutrients in the cave environment (Keeler and Lusk, 2021).

Metabolisms of microorganisms decay of guano and urea, and produce organic and inorganic acids, CO_2, H_2S, NH_3, and large amounts of microorganisms disperse into the cave air (Onac et al., 2009; De Waele et al., 2016; Armstrong et al., 2018). These components can also rise through warm air convection produced by exothermic guano breakdown or bat colonies and strongly erode walls and ceilings above the guano accumulation (e.g., Onac, 2019), similar to Fig. 1E in the bat hall.

One of the chemical reactions from distinct ecological cave zones is the precipitation of phosphorus-rich minerals. That may happen in guano deposits by bacteria, similar to those processes at the surface of organic-rich sediment located off Namibia by giant *Thiomaragarita namibiensis* bacteria (Schulz and Schulz, 2005).

Algae in the Karaftu Cave are cyanobacteria and diatoms (Fig. 13A- C), similar to those in Oregon Caves National Monument, Oregon, and Kauai Cave, Hawaii (Fig. 53 in St. Clair et al., 1981 and Figs. 21–23 in Miscoe et al., 2016, respectively). They can grow in the deep zones of the cave by changing the process from photosynthesis to chemosynthesis or increasing the number of thylakoids (Dove et al., 2006). Diatom, the predominant algae, can live in cave environments with low light and nutrient-dense (Romero, 2009). They are effective in nitrification if abundant (Pohlman et al., 1997).

Nitrosomonas sp. bacteria activity converts ammonia to nitrate (Kumaresan et al., 2015; Lavoie et al., 2015), releasing heat and generating hot spots in guano (Dumitraş and Marincea, 2021). That causes water to evaporate and form nitrate (Northup and Lavoie, 2001; Onac and Forti, 2011)/nitro mineral (Lavoie et al., 2015). By sulfo-oxidant bacteria in warm and wet conditions, H_2S transforms into sulfuric acid (e.g., van den Ende and van Gemerden, 1993) and, after reacts with $CaCO_3$, it precipitates gypsum (e.g., Kirkland, 2014) in guano accumulation.

Guano is a significant source of fungi that are mainly pathogenic (Dimkić et al., 2021). Some fungi cause several health-related problems among humans, such as *Histoplasma* (e.g., Emmons, 1949), which occurs in caves inhabited by bat guano (e.g., Lottenberg et al., 1979). Histoplasmosis spreads through spores or fungal elements suspended in dust particles and inhaled. Bat guano is also a natural reservoir of several viruses, such as COVID-19 (Dimkić et al., 2021) and SARS-CoV-2 pandemics (Temmam et al., 2022) (Fig. 13D, E). Therefore, communities living near guano should be careful about their health and safety.

Samples also contain high-level chitin (Fig. 13F), a biopolymer that forms the exoskeleton of arthropods and finds in the cell wall of fungi (e.g., Wurster et al., 2010; Dimkić et al., 2021). It is a resistant organic matter, even in acidic environments, and is more economically valuable than guano (Kaya et al., 2014).

4.7. Environmental hazards

The uneven floor of Karaftu Cave has led to the formation of water ponds of various sizes and shapes in the bat hall. Interaction between water and guano changes water chemistry during its residence in the cave and forms an acidic solution (pH = 5.6). It leads to the bedrock's dissolution, increasing the depth of the pond (Fig. 14A, B) and dissolve the substrate by passing water through that (Simon et al., 2007; 2010). It may be the beginning of the collapse of the cave floor and the generation of a new underground similar to the previous one in the bat hall (Figs. 1B, 14C). Environmental effects of this fall are a decrease in the groundwater level, change in the groundwater drainage system, drying of springs around the cave, loss of green cover, and a negative impact on the ecosystem in the region.

The groundwater from Karaftu Cave creates two springs that are the source of drinking water in the area. They dissolve the components inside the cave and their path. During their appearance outside the cave, like springs, they react with oxygen, their pH change from acidic to alkaline. In this case, some parts of the water-soluble matter precipitate as sludge in the small artificial pond outside the cave. Analysis show Ni (0.06 ppm), As (0.09 ppm), Pb (0.2 ppm), NO_3^-, and microorganisms pollutants in the water.

Microorganisms' contamination of water is the most dangerous type of pollution, and the most abundant and problematic factor is Animals' droppings, herein bat guano deposits. The decomposition of guano consumes water oxygen and introduces a variety of compounds into the water, such as nitrates, sulfates, and phosphates. These compounds are environmentally unfriendly, highly susceptible to spreading diseases, reduce water quality, increase groundwater acidity, and dissolve bedrock as they pass beneath guano deposits (Fig. 12).

5. Conclusions

Radiocarbon dating indicates that the accumulation of studied guano began at approximately 14260 ± 50 years BP after the LMG, with an average rate of 4.1 mm/year for depths of 360 to 205 cm.

Variations in the distribution of trace elements plus REEs and secondary minerals in guano deposits can provide good evidence for local paleoenvironmental and paleoclimate conditions. The Karafto Cave guano deposits reveal three paleoclimatic conditions, dry, wet, and dry terms, have been identified during its accumulation in Karafto Cave. Secondary minerals are taranakite, francoanellite, spheniscidite, whitlockite, pyrocoproite, brushite, leucophosphite, urea, niter, cesanite, and gypsum. The results in the studied profile show taranakite occur only in wet conditions, but whitlockite, urea, and cesanite exist just in dry ones. Therefore, these minerals can be an indicator of climate, but other minerals (because they are in both conditions) cannot be so.

This study shows that the Ce/Ce* and the correlation coefficient between Ce and Mn are good indicators for determining the local climatic conditions in guano deposits.

There are different sizes and shapes of water ponds in Karaftu Cave. Interaction between water and guano changes water chemistry during its residence in the cave and forms an acidic solution. As a result, the bedrock and the subsurface are dissolved by water seepage. That causes the cave to collapse and create a new underground similar to the previous underground in the bat hall. The falling of the cave floor leads to a decrease in the water table, changes in the groundwater drainage system, drying of springs around the cave, loss of green cover, and a negative impact on the ecosystem.

Leaching of the guano deposits by groundwater has increased the concentration of some trace elements and microorganisms in springs, close to Karaftu Cave, which poses pollution risks for man and the environment.

To keep the cave environment clean and remove these problems, it is better to harvest guano deposits and use them as fertilizer due to their importance in agriculture.

Declarations

Statement:

Research data related to the article is available in the master science thesis (in Persian with English abstract) of Ms. Haghighat jou and can be accessed from Irandoc.

Authors' Contributions:

Hadi Amin Rasouli carried out field geology, SPSS, and Excel, wrote the manuscript, and prepared the figures.

Masayo Minami performed carbon-14 analysis at Nagoya University and calibrated the age.

John Armstrong-Altrin reviewed the manuscript and his advice helped to improve the manuscript.

Nasim Haghighat Jou, Her master's thesis is a part of the manuscript.

Mehdi Moradi conducted ICP-MS analyses at the Geological Survey of Iran.

All named authors read the manuscript.

Funding:

We did not have any special financial aid for this study.

References

1. Albarede, F. (2011). Cerium (Anomalies of). In: M. Gargaud, R. Amils, J.C. Quintanilla, H.J. Cleaves, W.M. Irvine, D.L. Pinti, & M. Viso (eds.), Encyclopedia of Astrobiology. Springer Berlin Heidelberg, Berlin, Heidelberg. DOI: 10.1007/978-3-642-11274-4_260
2. Alibo, D.S., & Nozaki, Y. (1999). Rare earth elements in seawater: particle association, shale-normalization, and Ce oxidation. Geochimica et Cosmochimica Acta, 63 (3–4), 363–372. DOI: 10.1016/S0016-7037(98)00279-8
3. Amin-Rasouli, H., Haghighat jou, N., & Moradi, M. (2021). Geochemistry and ^{14}C dating of bat guano deposits from Karafto Cave, Divandareh, Kurdistan Province. Scientific Quarterly Journal of Geosciences, 31 (2), 21–30 (in Persian with English abstract). DOI: 10.22071/gsj.2020.220928.1762
4. Amin-Rasouli, H., Haghighat jou, N., & Moradi, M. (2022). Secondary minerals in the bat guano deposits from Karaftu Cave, Divandareh, Kurdistan province. Scientific Quarterly Journal of Geosciences, 32 (2), 75–88 (in Persian with English abstract). DOI: 10.22071/gsj.2021.286204.1909
5. Armstrong-Altrin, J.S. (2020). Detrital zircon U-Pb geochronology and geochemistry of the Riachuelos and Palma Sola beach sediments, Veracruz State, Gulf of Mexico: a new insight on palaeoenvironment. Journal of Palaeogeography, 9 (4), article no. 28. DOI: 10.1186/s42501-020-00075-9.
6. Armstrong-Altrin, J.S., & Machain-Castillo, M.L. (2016). Mineralogy, geochemistry, and radiocarbon ages of deep sea sediments from the Gulf of Mexico, Mexico. Journal of South American Earth Sciences, vol. 71, pp. 182–200. DOI: 10.1016/j.jsames.2016.07.010
7. Armstrong-Altrin, J.S., Madhavaraju, J., Vega-Bautista, F., Ramos-Vázquez, M.A., Pérez-Alvarado, B.Y., Kasper-Zubillaga, J.J., & Ekoa Bessa, A.Z. (2021). Mineralogy and geochemistry of Tecolutla and Coatzacoalcos beach sediments, SW Gulf of Mexico. Applied Geochemistry. 134, 105103 DOI: 10.1016/j.apgeochem.2021.105103.
8. Armstrong-Altrin, J.S., Ramos-Vázquez, M.A., Madhavaraju, J., Marca-Castillo, M.E., Machain-Castillo, M.L., & Márquez-Garcia, A.Z. (2022). Geochemistry of marine sediments adjacent to the Los Tuxtlas Volcanic Complex, Gulf of Mexico: Constraints on weathering and provenance. Applied Geochemistry, 141, no. 105321. DOI: 10.1016/j.apgeochem.2022.105321.
9. Armstrong, P., Beard, J., Bonilla, L., Arboleda, N., Lindsley, M., Chae, S., Castillo, D., Nuñez, R., Chiller, T., De Perio, M., Pimentel, R., & Vallabhaneni, S. (2018). Outbreak of severe histoplasmosis among tunnel workers-Dominican Republic, 2015. Clinical Infectious Diseases, 66, 1550–1557. DOI: 10.1093/cid/cix1067
10. Audra, P., Bosák, P., Gázquez, F., Cailhol, D., Skála, R., Lisá, L., Jonášová, Š., Frumkin, A., Knez, M., Slabe, T., Zupan Hajna, N., & Al-Farraj, A. (2017). Bat urea-derived minerals in arid environment. First identification of allantoin, $C_4H_6N_4O_3$, in Kahf Kharrat Najem Cave, United Arab Emirates. International Journal of Speleology, 46, 81–92. DOI: 10.5038/1827-806X.46.1.2001
11. Audra, P., Heresanu, V., Barriquand, L., Boutchich, M.E.K., Jaillet, S., Pons-Branchu, E., Bosák, P., Cheng, H., Edwards, R.L., & Renda, M. (2021). Bat guano minerals and mineralization processes in chameau cave, Eastern Morocco. International Journal of Speleology, 50, 91–109. DOI: 10.5038/1827-806X.50.1.2374
12. Batina, M.C., & Reese, C.A. (2011). A Holocene pollen record recovered from a guano deposit: Round Spring Cavern, Missouri, USA. Boreas, 40, 332–341. DOI: 10.1111/j.1502-3885.2010.00186.x
13. Bau, M. (1999). Scavenging of dissolved yttrium and rare earths by precipitating iron oxyhydroxide: experimental evidence for Ce oxidation, Y-Ho fractionation, and lanthanide tetrad effect. Geochimica et Cosmochimica Acta, 63(1), 67–77. DOI: 10.1016/S0016-7037(99)00014-9
14. Bau, M., & Dulski, P. (1996). Distribution of yttrium and rare-earth elements in the Penge and Kuruman iron-formations, Transvaal Supergroup, South Africa. Precambrian Research, 79, 37–55. DOI: 10.1016/0301-9268(95)00087-9
15. Benda, P., Faizolâhi, K. Andreas, M., Obuch, J., Reiter, A., Ševčík, M., Uhrin, M., Vallo, P., & Ashrafı, S. (2012). Bats (Mammalia: Chiroptera) of the Eastern Mediterranean and Middle East. Part 10. Bat fauna of Iran. Acta Societatis Zoologicae Bohemicae, 76, 163–582. ISSN: 1211-376X
16. Bird, M.I., Boobyer, E.M., Bryant, C., Lewis, H.A., Paz, V., & Stephens, W.E. (2007). A long record of environmental change from bat guano deposits in Makangit Cave, Palawan, Philippines. Earth and Environmental Science Transactions of the Royal Society of Edinburgh, 98, 59–69. DOI: 10.1017/s1755691007000059
17. Bozorgnia, F. (1965). Qom Formation stratigraphy of the Central Basin of Iran and its intercontinental position. Bulletin of the Iranian Petroleum Institute, 24, 69–75.
18. Brauer, A., Endres, C., Günter, C., Litt, T., Stebich, M., & Negendank, J.F.W. (1999). High resolution sediment and vegetation responses to Younger Dryas climate change in varved lake sediments from Meerfelder Maar, Germany. Quaternary Science Reviews, 18, 321–329. DOI: 10.1016/S0277-3791(98)00084-5
19. Bridge, P. (1973). Guano minerals from Murra-el-elevyn Cave, Western Australia. Mineralogical Magazine, 39, 346–348. DOI: 10.1180/minmag.1973.039.303.11
20. Cañaveras, J.C., Sanchez-Moral, S., Soler, V., & Saiz-Jimenez, C. (2001). Microorganisms and microbially induced fabrics in cave walls. Geomicrobiology Journal, 18, 223–240. DOI: 10.1080/01490450152467769
21. Cleary, D., Onac, B., Tanţău, I., Forray, F., Wynn, J., Ionita, M., & Tămaş, T. (2018). A guano-derived $\delta^{13}C$ and $\delta^{15}N$ record of climate since the Medieval Warm Period in north-west Romania. Journal of Quaternary Science, 33, 677–688. DOI: 10.1002/jqs.3044
22. Cleary, D., Feurdean, A., Tanţău, I., & Forray, F. (2019). Pollen, $\delta^{15}N$ and $\delta^{13}C$ guano-derived record of late Holocene vegetation and climate in the southern Carpathians, Romania. Review of Palaeobotany and Palynology, 265, 62–75. DOI: 10.1016/j.revpalbo.2019.03.002

23. Cleary, D.M., & Onac, B.P. (2021). Using ratios in cave guano to assess past environmental changes. Geological Society, London, Special Publications, 507, 209–224. DOI: 10.1144/SP507-2020-13
24. Cuculić, V., Cukrov, N., Kwokal, Ž., & Mlakar, M. (2011). Distribution of trace metals in anchialine caves of Adriatic Sea, Croatia. Estuarine, Coastal and Shelf Science, 95, 253–263. DOI: 10.1016/j.ecss.2011.09.011
25. Cuezva, S., Sanchez-Moral, S., Saiz-Jimenez, C., & Canaveras, J.C. (2009). Microbial communities and associated mineral fabrics in Altamira cave, Spain. International Journal of Speleology, 38, 83–92. DOI: 10.5038/1827-806X.38.1.9
26. Cuffey, K.M., & Clow, G.D. (1997). Temperature accumulation and ice sheet elevation in central Greenland through the last deglacial transition. Journal of Geophysical Research, 102, 26383–26396. DOI: 10.1029/96JC03981
27. Culver, D.C., & Pipan, T. (2019). The Biology of Caves and Other Subterranean Habitats. Oxford University Press, 256. DOI: 10.1093/oso/9780198820765.001.0001
28. De Baar, H.J., German, C.R., Elderfield, H., & van Gaans, P. (1988). Rare earth element distributions in anoxic waters of the Cariaco Trench. Geochimica et Cosmochimica Acta, 52, 1203–1219. DOI: 10.1016/0016-7037(88)90275-X
29. De Carlo, E.H., & Green, W.J. (2002). Rare earth elements in the water column of Lake Vanda, McMurdo Dry Valleys, Antarctica. Geochimica et Cosmochimica Acta, 66, 1323–1333. DOI: 10.1016/S0016-7037(01)00861-4
30. De Carlo, E.H., Wen, X.Y., & Irving, M. (1997). The influence of redox reactions on the uptake of dissolved Ce by suspended Fe and Mn oxide particles. Aquatic Geochemistry, 3, 357–389. DOI: 10.1023/A:1009664626181
31. De Waele, J., Audra, P., Madonia, G., Vattano, M., Plan, L., D'Angeli, I.M., Bigot, J.-Y., & Nobécourt, J.C. (2016). Sulfuric acid speleogenesis (SAS) close to the water table: Examples from southern France, Austria, and Sicily. Geomorphology, 253, 452–467. DOI: 10.1016/j.geomorph.2015.10.019
32. Dimkić, I., Stanković, S., Kabić, J., Stupar, M., Nenadić, M., Ljaljević-Grbić, M., Žikić, V., Vujisić, L., Tešević, V., Vesović, N., Pantelić, D., Savić-Šević, S., Vukojević, J., & Ćurčić, S. (2020). Bat guano-dwelling microbes and antimicrobial properties of the pygidial gland secretion of a troglophilic ground beetle against them. Applied Microbiology and Biotechnology, 04(9), 4109–4126. DOI: 10.1007/s00253-020-10498-y
33. Dimkić, I., Fira, D., Janakiev, T., Kabić, J., Stupar, M., Nenadić, M., Unković, N., & Grbić, M.L. (2021). The microbiome of bat guano: for what is this knowledge important? Applied microbiology and biotechnology, 105, 1407–1419. DOI: 10.1007/s00253-021-11143-y
34. Dodge-Wan, D., Viswanathan, P.M., Ramasamy, N., & Arumugam, A. (2017). Epiphreatic caves in Niah karst tower (NW Borneo): occurrence, morphology and hydrogeochemistry. Acta Carsologica, 46, 149–163. DOI: 10.3986/ac.v46i2-3.4935
35. Dove, S., Ortiz, J.C., Enriquez, S., Fine, M., Fisher, P., Iglesias-Prieto, R., Thornhill, D., & Hoegh-Guldberg, O. (2006). Response of holosymbiont pigments from the scleractinian coral Montipora monasteriata to short-term heat stress. Limnology and Oceanography, 51, 1149–1158. DOI: 10.4319/lo.2006.51.2.1149
36. Dumitraş, D., & Marincea, Ş. (2021). Sequential dehydration of the phosphate–sulfate association from Gura Dobrogei Cave, Dobrogea, Romania. European Journal Mineralogy, 33, 329–340. DOI: 10.5194/ejm-33-329-2021
37. Emmons, C.W. (1949). Isolation of Histoplasma capsulatum from soil. Public Health Report, 64, 892–896. DOI: 10.2307/4587021
38. Forray, F.L., Onac, B.P., Tanţău, I., Wynn, J.G., Tămaş, T., Coroiu, I., & Giurgiu, A.M. (2015). A Late Holocene environmental history of a bat guano deposit from Romania: an isotopic, pollen and microcharcoal study. Quaternary Science Reviews, 127, 141–154. DOI: 10.1016/j.quascirev.2015.05.022
39. Forti, P. (2001). Biogenic speleothems: an overview. International Journal of Speleology, 30 (1/4), 39–56. DOI: 10.5038/1827-806X.30.1.4
40. Forti, P., Galli, E., Rossi, A., Pint, J., & Pint, S. (2004). Ghar Al Hibashi Lava Tube: The Richest Site in Saudi Arabia for Cave Minerals. Acta Carsologica, 33, 189–205. DOI: 10.3986/ac.v33i2.299
41. Gangloff, S., Stille, P., Schmitt, A.D., & Chabaux, F. (2016). Factors controlling the chemical composition of colloidal and dissolved fractions in soil solutions and the mobility of trace elements in soils. Geochim. Cosmochim. Acta 189, 37–57. DOI: 10.1016/j.gca.2016.06.009
42. Giurgiu, A., & Tamas, T. (2013). Mineralogical data on bat guano deposits from three Romanian caves. Studia Universitatis Babes-Bolyai Geologia, 58(2), 13–18. DOI: 10.5038/1937-8602.58.2.2
43. Haghighat jou, N. (2017). Geochemistry of guano deposits of Karaftu Cave, Divandareh, Iran. M.Sc. thesis, University of Kurdistan, 74p (in Persian with English abstract).
44. Haluschak, P., Eilers, R.G., Mills G.F., & Grift, S. (1998). Status of Selected Trace Elements in Agricultural Soils of Southern Manitoba. Technical Bulletin 1998-6E Cat. No. A54-8/1998-6E ISBN 0-662-27098-3.
45. Hill, C.A., & Forti, P. (1997). Cave minerals of the world. 2nd ed., Huntsville, National Speleological Society, 464 p.
46. Johnston, V.E., McDermott, F., & Tămaş, T. (2010). A radiocarbon dated bat guano deposit from NW Romania. Implications for the timing of the Little Ice Age and Medieval Climate Anomaly. Palaeogeography, Palaeoclimatology, Palaeoecology, 291, 217–227. DOI: 10.1016/j.palaeo.2010.02.031
47. Kabata-Pendias, A. (2010). Trace Elements in Soils and Plants (4th ed.). CRC Press. DOI: 10.1201/b10158
48. Karkanas, P., Rigaud, J.P., Simek, J.F., Albert, R.M., & Weiner, S. (2002). Ash bones and guano: a study of the minerals and phytoliths in the sediments of Grotte XVI, Dordogne, France. Journal of Archaeological Science, 29(7), 721–732. DOI: 10.1006/jasc.2001.0742
49. Kato, Y., Fujinaga, K., Nakamura, K., Takaya, Y., Kitamura, K., Ohta, J., Toda, R., Nakashima, T., & Iwamori, H. (2011). Deep-sea mud in the Pacific Ocean as a potential resource for rare-earth elements. Nature Geoscience, 4, 535–539. DOI: 10.1038/ngeo1185
50. Kaya, M., Seyyar, O., Baran, T., & Turkes, T. (2014). Bat guano as new and attractive chitin and chitosan source. Frontiers in Zoology, 11, 59–66. DOI: 10.1186/s12983-014-0059-8
51. Keeler, R., & Lusk, B. (2021). Microbiome of Grand Canyon Caverns, a dry sulfuric karst cave in Arizona, supports diverse extremophilic bacterial and archaeal communities. Journal of Cave and Karst Studies, 83, 44–56. DOI: 10.4311/2019MB0126

52. Kholghi Khasraghi, M.H. (1999). Irankhah Geological Map 1:100000. Geological survey of Iran.
53. Kirkland, D.W. (2014). National Cave and Karst Research Institute Special Paper 2: Role of Hydrogen Sulfide in the Formation of Cave and Karst Phenomena in the Guadalupe Mountains and Western Delaware Basin, New Mexico and Texas. Carlsbad (NM): National Cave and Karst Research Institute. http://scholarcommons.usf.edu/tles_pub/3
54. Kumaresan, D., Hillebrand-Voiculescu, A.M., Wischer, D., Stephenson, J., Chen, Y., Murrell, J.C. (2015). Microbial life in unusual cave ecosystems sustained by chemosynthetic primary production. In: A.S. Engel (ed.), Life in extreme environments: microbial life of cave systems. DeGruyter, Berlin, 215–230 pp. DOI: 10.1515/9783110339888
55. Lavoie, K.H. (2015). A grand, gloomy, and peculiar place: microbiology in the Mammoth Cave region. In: A.S. Engel (ed.), Life in extreme environments: microbial life of cave systems. DeGruyter, Berlin, 47–78 pp. DOI: 10.1515/9783110339888-005
56. Ling, S., Wu, X., Ren, Y., Sun, C., Xin Liao, X., Li, X., & Zhu, B. (2015). Geochemistry of trace and rare earth elements during weathering of black shale profiles in Northeast Chongqing, Southwestern China: Their mobilization, redistribution, and fractionation. Geochemistry, 75 (3), 403–417. DOI: 10.1016/j.chemer.2015.07.004
57. Lottenberg, O., Waldman, R.H., Ajello, L., Hoff, G.L., Bigler, W., & Zellner, S.R. (1979). Pulmonary histoplasmosis associated with exploration of a bat cave. The American Journal of Epidemiology, 110, 156–161. DOI: 10.1093/oxfordjournals.aje.a112800
58. McLennan, S.M. (1989). Rare earth elements in sedimentary rocks; influence of provenance and sedimentary processes. Reviews in Mineralogy and Geochemistry, 21, 169–200. Available at: http://rimg.geoscienceworld.org/content/21/1/169.s
59. Miscoe, L.H., Johansen, J., Kociolek, J., Lowe, R., Vaccarino, M.A., Pietrasiak, N., & Sherwood, A. (2016). The diatom flora and cyanobacteria from caves on Kauai, Hawaii. Bibliotheca Phycologica, 120, 3–74.
60. Mohajjel, M., Fergusson, C.L., & Sahandic, M.R. (2003). Cretaceous-Tertiary Convergence and Continental Collision Sanandaj-Sirjan Zone, Western Iran. Journal of Asian Earth Sciences, 21, 397–412. DOI: 10.1016/S1367-9120(02)00035-4
61. Nakada, R., Shibuya, T., Suzuki, K., & Takahashi, Y. (2017). Europium anomaly variation under low-temperature water-rock interaction: A new thermometer. Geochemistry International, 55, 822–832. DOI: 10.1134/S001670291709004X
62. Northup, D.E., & Lavoie, K.H. (2001). Geomicrobiology of caves: A review. Geomicrobiology Journal, 18(3), 199–220. DOI: 10.1080/01490450152467750
63. Obaje, S.O., Akpoborie, I.A., Ugbe, F.C., & Onugba, A. (2015). Rare Earth and Trace Elements Distribution in Sediments of River Gora, Minna Area, North-Central Nigeria: Implication for Provenance. Earth Science Research, 4, 1–10. DOI: 10.5539/esr.v4n1p103
64. Ohta, A., & Kawabe, I. (2001). REE (III) adsorption onto Mn dioxide (δ-MnO_2) and Fe oxyhydroxide: Ce (III) oxidation by δ-MnO_2. Geochimica et Cosmochimica Acta, 65(5), 695–703. DOI: 10.1016/S0016-7037(00)00578-0
65. Onac, B.P. (2019). Cave discovered by mining activities and mined caves. In: G.M.L. Ponta, B.P. Onac (eds.), Cave and karst systems of Romania. Springer International, Cham, 475–483 pp. DOI: 10.1007/978-3-319-90747-5_54
66. Onac, B.P., & Veres, D. (2003). Sequence of secondary phosphates deposition in a karst environment: evidence from Magurici Cave (Romania). European Journal of Mineralogy, 15, 741–745. DOI: 10.1127/0935-1221/2003/0015-0741
67. Onac, B.P., & Forti, P. (2011). Mineralogenetic mechanisms occurring in the cave environment: an overview. International Journal of Speleology, 40 (2), 79–98. DOI: 10.5038/1827-806X.40.2.1
68. Onac, B.P., Breban, R., Kearns, J., & Timat, T. (2002). Unusual minerals related to phosphate deposits in Cioclovina Cave, Sureanu Mts. (Romania). Theoretical and Applied Karstology, 15, 27–34. https://digitalcommons.usf.edu/geo_facpub/778
69. Onac, B.P., Sumrall, J., Mylroie, J.E., & Kearns, J.B. (2009). Cave Minerals of San Salvador Island, Bahamas. 15th International Congress of Speleology, Book 1, 318–323 pp. Available at: http://scholarcommons.usf.edu/tles_pub/1
70. Onac, B.P., Forray, F., Wynn, J.G., & Giurgiu, A.M. (2014). Guano-derived $\delta^{13}C$-based on paleo-hydroclimate record from Gaura cu Musca Cave, SW Romania. Environmental Earth Science, 71, 4061–4069. DOI: 10.1007/s12665-013-2789-x
71. Plan, L., Tschegg, C., De Waele, J., & Spötl, C. (2012). Corrosion morphology and cave wall alteration in an Alpine sulfuric acid cave (Kraushöhle, Austria). Geomorphology, 169, 45–54. DOI: 10.1016/j.geomorph.2012.04.006
72. Pohlman, J.W., Iliffe, T.M., & Cifuentes, L.A. (1997). A stable isotope study of organic cycling and the ecology of an anchialine cave ecosystem. Marine Ecology Progress Series, 155, 17–27. DOI: 10.3354/meps155017
73. Ramos-Vázquez, M.A., Armstrong-Altrin, J.S., Machain-Castillo, M.L., & Gío-Argáez, F.R. (2018). Foraminiferal assemblages, ^{14}C ages, and compositional variations in two sediment cores in the western Gulf of Mexico. Journal of South American Earth Sciences, Vol. 88, pp. 480–496.
74. Ramos-Vázquez, M.A., Armstrong-Altrin, J.S., Madhavaraju, J., Gracia, A., & Salas-de-León, D.A. (2022). Mineralogy and geochemistry of marine sediments in the Northeastern Gulf of Mexico. In: Armstrong-Altrin JA, Pandarinath K, & Verma S. (Eds.), Geochemical Treasures and Petrogenetic Processes. P. 153–183. DOI: 10.1007/978-981-19-4782-7_7
75. Reimer, P.J., Bard, E., Bayliss, A., Beck, J.W., Blackwell, P.G., Ramsey, C.B., Buck, C.E., Cheng, H., Edwards, R.L., Friedrich, M., Grootes, P.M., Guilderson, T.P., Haflidason, H., Hajdas, I., Hajdas, C., Heaton, T.J., Hoffmann, D.L., Hogg, A.G., Hughen, K.A., Kaiser, K.F., Kromer, B., Manning, S.W., Niu, M., Reimer, R.W., Richards, D.A., Scott, E.M., Southon, J.R., Staff, R.A., Turney, C.S.M., & van der Plicht, J. (2013). IntCal13 and Marine13 radiocarbon age calibration curves 0–50,000 years cal BP. Radiocarbon, 55(4), 1869–1887. DOI: 10.2458/azu_js_rc.55.16947
76. Riquier, L., Tribovillard, N., Averbuch, O., Devleeschouwer, X., & Riboulleau, A. (2006). The Late Frasnian Kellwasser horizons of the Harz Mountains (Germany): two oxygen-deficient periods resulting from contrasting mechanisms. Chemical Geology, 233: 137–155. DOI:10.1016/j.chemgeo.2006.02.021
77. Romero, Jr.A. (2009). Cave Biology: Life in Darkness. 1st ed., New York, Cambridge University Press, 306 pp.

78. Reuter, M., Piller, W.E., Harzhauser, M., Mandic, O., Berning, B., Rögl, F., Kroh, A., Aubry, M.-P., Wielandt-Schuster, U., & Hamedani, A. (2009). The Oligo-/Miocene Qom Formation (Iran): evidence for an early Burdigalian restriction of the Tethyan Seaway and closure of its Iranian gateways. International Journal of Earth Sciences, 98, 627–650. DOI: 10.1007/s00531-007-0269-9
79. Sakoui, S., Derdak, R., Addoum, B., Serrano-Delgado, A., Soukri, A., & El Khalfi, B. (2020). The Life Hidden Inside Caves: Ecological and Economic Importance of Bat Guano. International Journal of Ecology, Article ID 9872532, 2020, 1–7. DOI: 10.1155/2020/9872532
80. Schulz, H.N., & Schulz, H.D. (2005). Large sulfur bacteria and the formation of phosphorite. Science, 307(5708), 416–418. DOI: 10.1126/science.1103096
81. Shahack-Gross, R., Berna, F., Karkanas, P., & Weiner, S. (2004). Bat guano and preservation of archaeological remains in cave sites. Journal of Archaeological Science, 31(9), 1259–1272. DOI: 10.1016/j.jas.2004.02.004
82. Sholkovitz, E.R., Landing, W.M., & Lewis, B.L. (1994). Ocean particle chemistry: The fractionation of rare earth elements between suspended particles and seawater. Geochimica et Cosmochimica Acta, 58, 1567–1579. DOI: 10.1016/0016-7037(94)90559-2
83. Sanematsu, K., Kon, Y., Imai, A., Watanabe, K., & Watanabe, Y. (2013). Geochemical and mineralogical characteristics of ion-adsorption type REE mineralization in Phuket, Thailand. Mineralium Deposita, 48, 437–451. DOI: 10.1007/s00126-011-0380-5
84. Simon, K.S., Pipan, T., & Culver, D. (2007). A conceptual model of the flow and distribution of organic carbon in caves. Journal of Cave and Karst Studies, 69, 279–284.
85. Simon, K.S., Pipan, T., Ohno, T., & Culver, D.C. (2010). Spatial and temporal patterns in abundance and character of dissolved organic matter in two karst aquifers. Fundamental and Applied Limnology, 177, 81–92. DOI: 10.1127/1863-9135/2010/0177-0081
86. Smol, J.P., & Cumming, B.F. (2000). Tracking long-term changes in climate using algal indicators in lake sediments. Journal of Phycology, 36, 986–1011. DOI: 10.1046/j.1529-8817.2000.00049.x
87. Snow, M.R., Pring, A., & Allen, N. (2014). Minerals of the Wooltana Cave, Flinders Ranges, South Australia. Transactions of the Royal Society of South Australia, 138, 214–230. DOI: 10.1080/03721426.2014.11649009
88. St. Clair L.L., Rushforth, S.R., & Allen, J.V. (1981). Diatoms of Oregon Caves National Monument, Oregon. Great Basin Naturalist, 41(3), 317–332. Available at: https://scholarsarchive.byu.edu/gbn/vol41/iss3/9
89. Stöcklin, J. (1968). Structural history and tectonics of Iran: a review. American Association of Petroleum Geologists Bulletin, 52, 1229–1258. DOI: 10.1306/5D25C4A5-16C1-11D7-8645000102C1865D
90. Stöcklin, J., & Nabavi, M. (1972). Tectonic map of Iran, Scale 1:2500000. Geological Survey of Iran.
91. Street-Perrott, F.A., & Perrott., R.A. (1990). Abrupt climate fluctuations in the tropics: The influence of Atlantic Ocean circulation, Nature, 343, 607–612. DOI: 10.1038/343607a0
92. Taylor, S.R., & McLennan, S.M. (1985). The continental crust: its composition and evolution. Blackwell, Scientific Publication, Carlton, 312 pp.
93. Tazaki, K. (2006). Clays, microorganisms, and biomineralization. In: F. Bergaya, B.K.G. Theng, G. Lagaly (eds.), Handbook of clay science. Elsevier, Amsterdam, 477–497 pp.
94. Temmam, S., Vongphayloth, K., & Baquero, E., et al. (2022). Bat coronaviruses related to SARS-CoV-2 and infectious for human cells. Nature 604, 330–336. DOI: 10.1038/s41586-022-04532-4
95. Tostevin, R., Shields, G.A., Tarbuck, G.M., He, T., Clarkson, M.O., & Wood, R.A. (2016). Effective use of cerium anomalies as a redox proxy in carbonate-dominated marine settings. Chemical Geology, 438, 146–162. DOI: 10.1016/j.chemgeo.2016.06.027
96. Tribovillard, N., Algeo, T.J., & Lyons, T. (2006). Trace metals as paleoredox and paleoproductivity proxies: An update. Chemical Geology, 232: 12–32. DOI: 10.1016/j.chemgeo.2006.02.012
97. Tsalickis, A., Waters, M.N., & Campbell, J.W. (2021). Methods and analysis of bat guano cores from caves for paleoecology. Journal of Cave and Karst Studies, 83, 141–150. DOI: 10.4311/2020ES0104
98. van den Ende, F.P., & van Gemerden H. (1993). Sulfide oxidation under oxygen limitation by a Thiobacillus thioparus isolated from a marine microbial mat. FEMS Microbiol Ecol, 13, 69–78. https://www.sciencedirect.com/science/article/pii/0168649693900426
99. van Zeist, W., & Wright, H.E. Jr. (1963). Preliminary pollen studies at Lake Zeribar, Zagros Mountains, southwestern Iran. Science, 140, 63–67. DOI: 10.1016/0034-6667(67)90159-5
100. van Zeist, W., & Bottema, S. (1977). Palynological investigations in western Iran. Palaeohlistoria XIX, 19–85. DOI: 10.1191/0959683605hl846rp
101. Wells, S.G., Dunbar, N.W., & Timmons, J.M. (2022). New Mexico Earth Matter: New Mexico's Sulfuric Acid Caves. New Mexico Bureau of Geology and Mineral Resources, Institute of Mining and Technology, 22 (2), 1–6. https://geoinfo.nmt.edu/publications/periodicals/earthmatters/22/n2/em_v22_n2.pdf
102. Wurster, C.M., McFarlane, D.A., Bird, M.I., Ascough, P., & Athfield, N.B. (2010). Stable isotopes of subfossil bat guano as a long-term environmental archive: insights from a Grand Canyon cave deposit. Journal of Cave and Karst Studies, 72, 111–121. DOI: 10.4311/jcks2009es0109
103. Wurster, C.M., Munksgaard, N., Zwart, C., & Bird, M. (2015). The biogeochemistry of insectivorous cave guano: a case study from insular Southeast Asia. Biogeochemistry, 124 (1–3), 163–175. DOI: 10.1007/s10533-015-0089-0
104. Wurster, C.M., Rifai, H., Haig, J., Titin, J., Jacobsen, G., & Bird, M. (2017). Stable isotope composition of cave guano from eastern Borneo reveals tropical environments over the past 15,000 cal yr BP. Palaeogeography, Palaeoclimatology, Palaeoecology, 473, 73–81. DOI: 10.1016/j.palaeo.2017.02.029

Figures

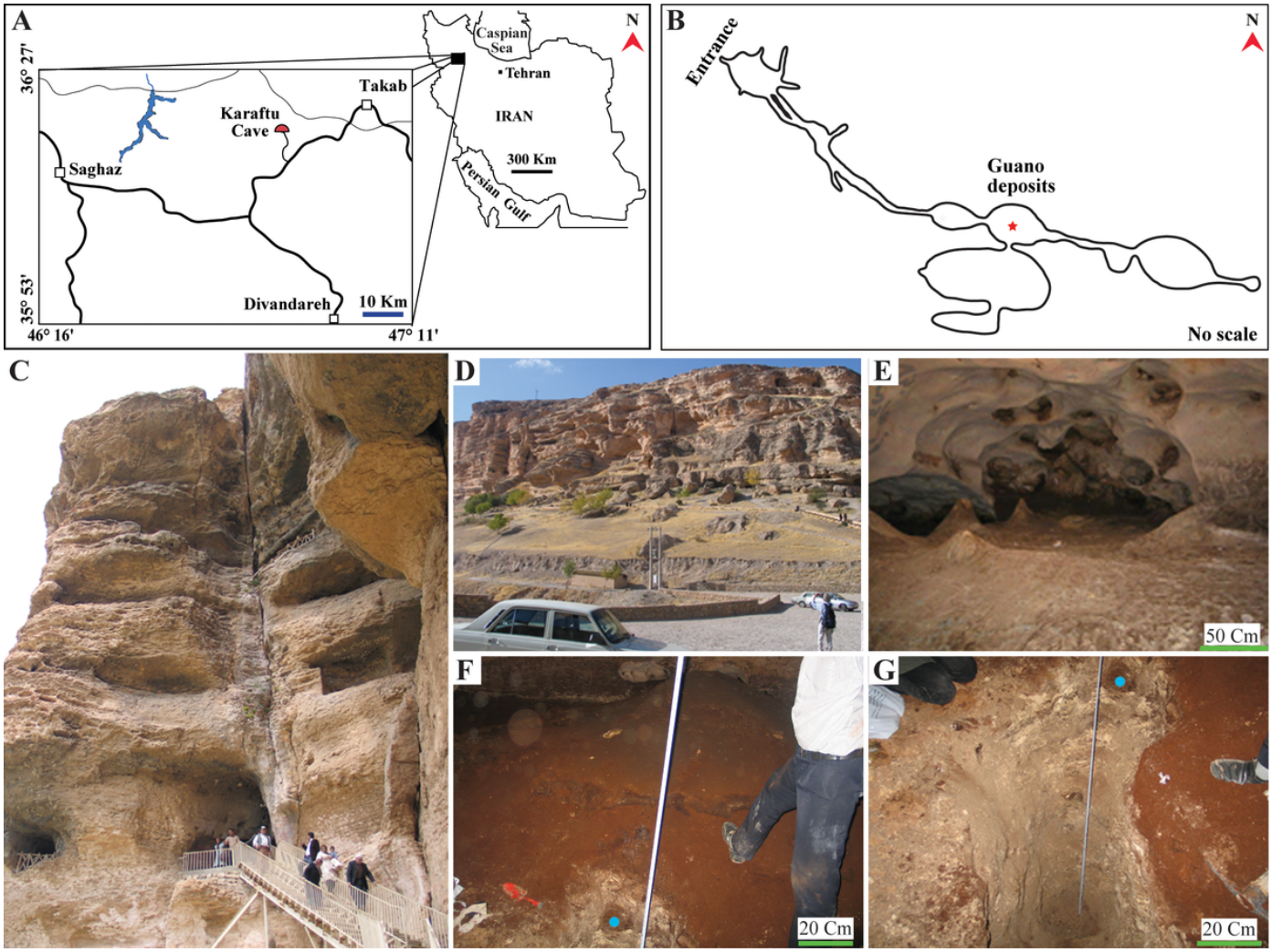

Figure 1

A) Location map of the study area. B) The guano deposits situation in the bat hall of the Karaftu Cave (* = the sampling points). C) A view (to NE) of the entrance of Karaftu Cave. D) Panorama of Karaftu Cave, view to NE. E) Guano deposits in the bat hall. F, G) Photos showing the pit dug through the studied bat guano for sampling. The blue circles represent the same point in Figures F and G.

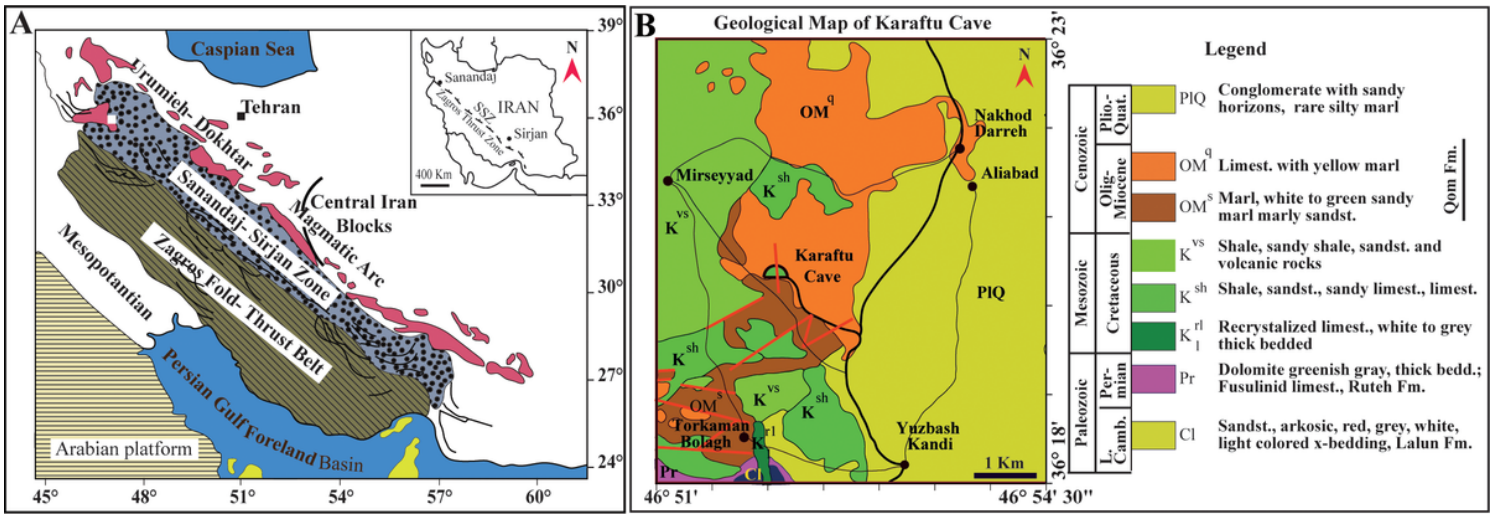

Figure 2

A) Map of Iran showing major tectonic plates plus associated boundaries and the location of Sanandaj-Sirjan Zone between Zagros Fold-Thrust belt and Urumieh-Dokhtar magmatic arc (Stöcklin and Nabavi, 1972). B) Geological map of the Karaftu area (after Kholghi Khasraghi, 1999).

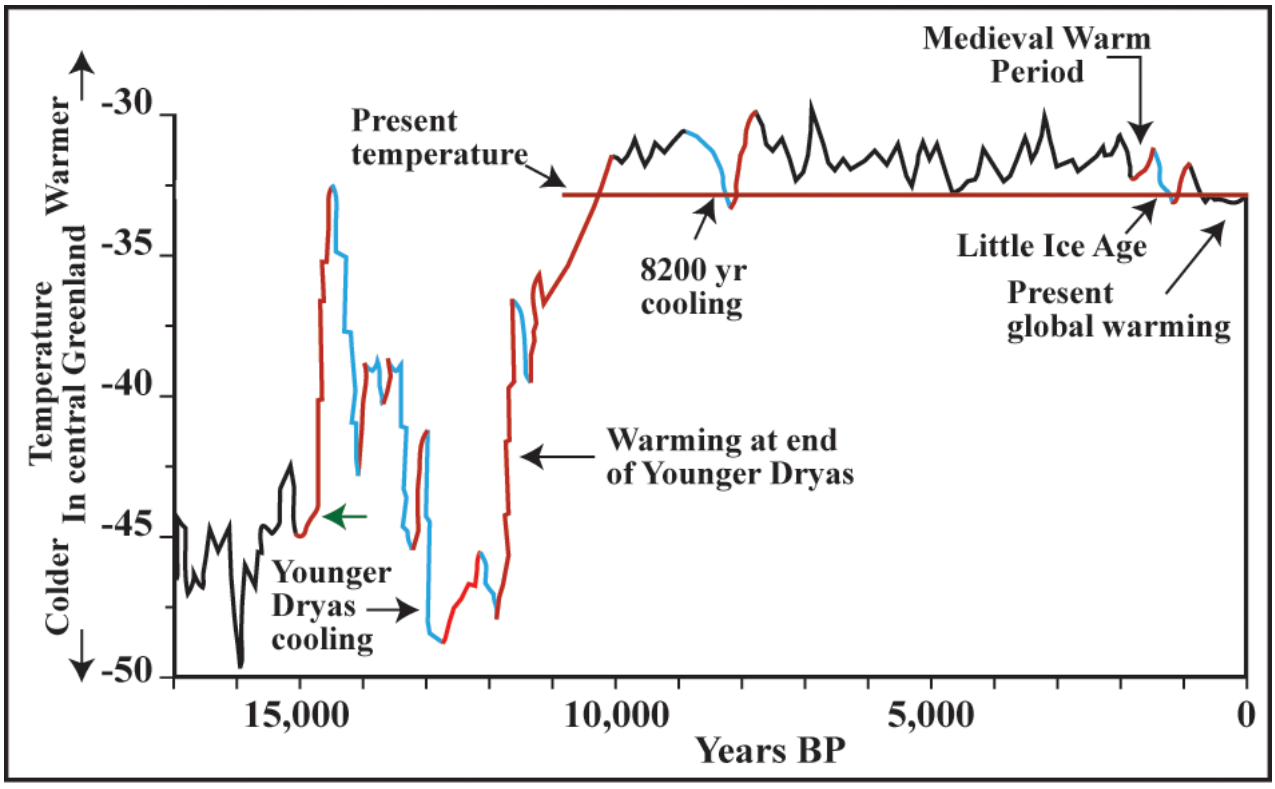

Figure 3

Determination of paleoclimate based on ^{14}C dating (Cuffey and Clow, 1997). The diagram shows the LGM of about 16,000 years BP. The green arrow represents the onset of guano accumulation in the bat hall, Karaftu Cave.

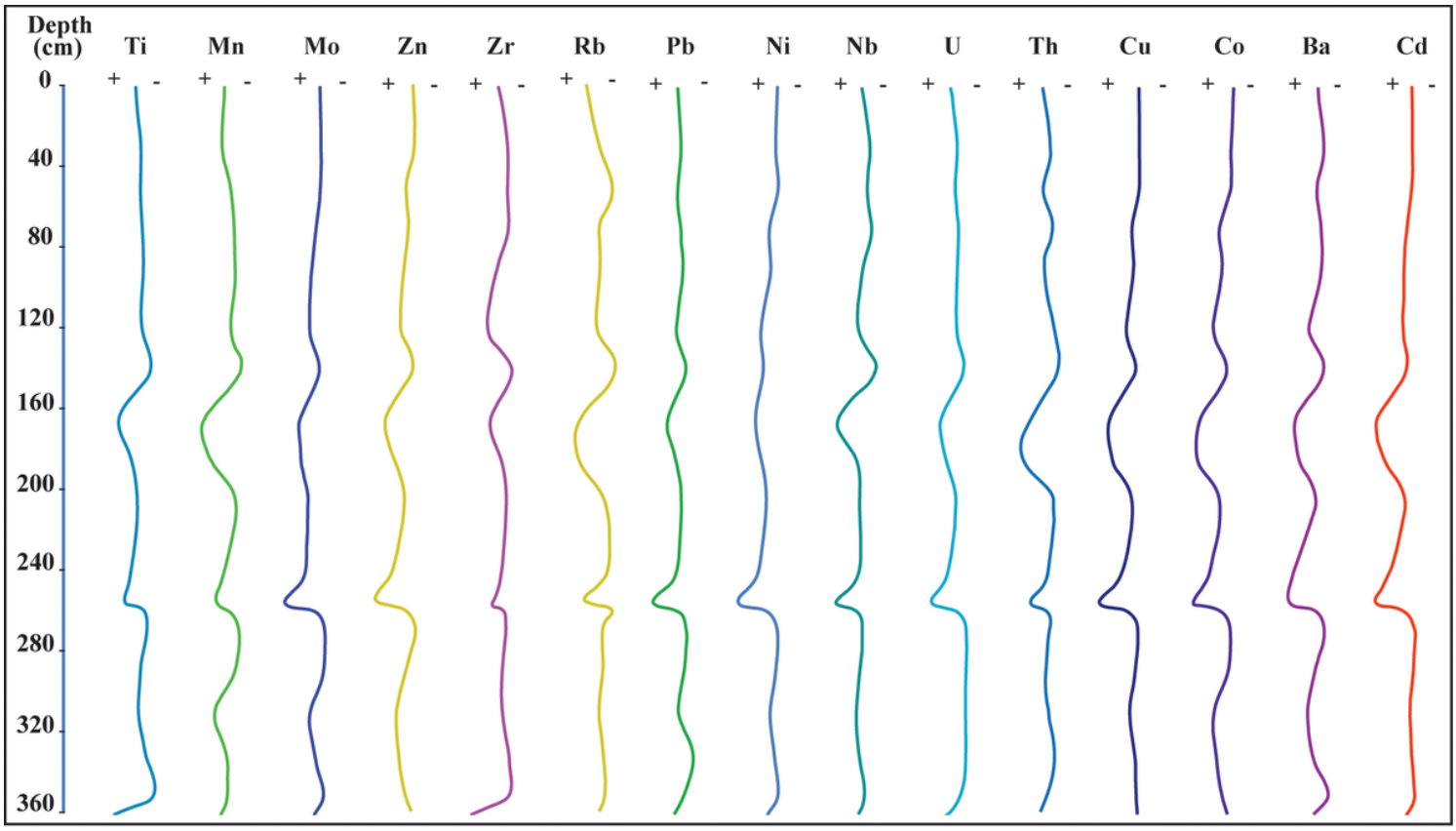

Figure 4

Distribution trends of trace elements along depth in the guano profile of Karaftu Cave. The high abundances of Ti and Zr at the base of the guano profile are due to the low rate of guano accumulation. The symbols + and – indicate the increase and decrease of the values of elements, respectively. High concentrations of elements indicate wet conditions along the profile (Amin-Rasouli et al., 2021).

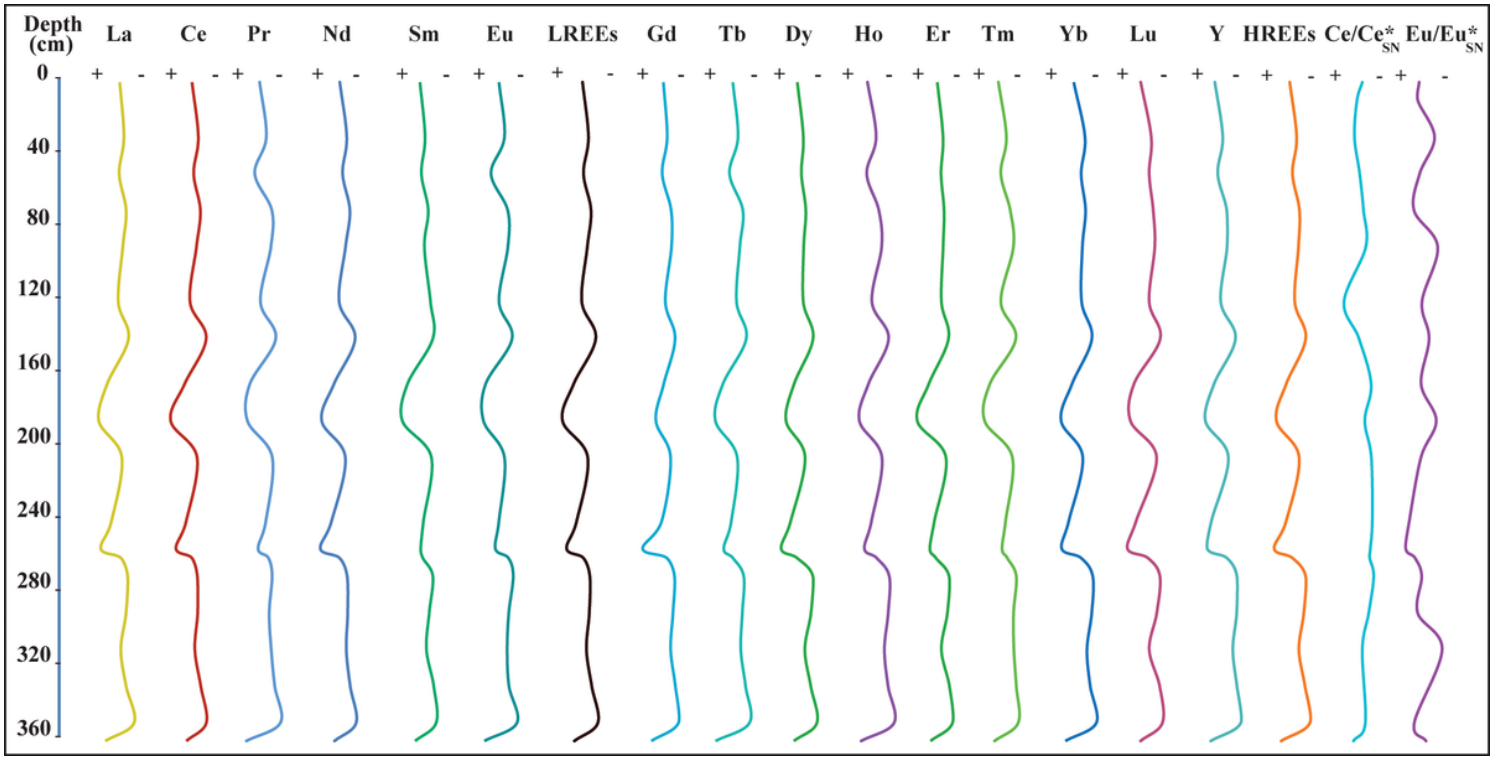

Figure 5

The distribution of REEs indicates three main units/climate changes through the guano profile (excluding the Eu/Eu^*_{SN} pattern). The symbols + and – represent the increase and decrease of the values of elements, respectively. High concentrations of elements indicate wet conditions along the profile (Amin-Rasouli et al., 2021).

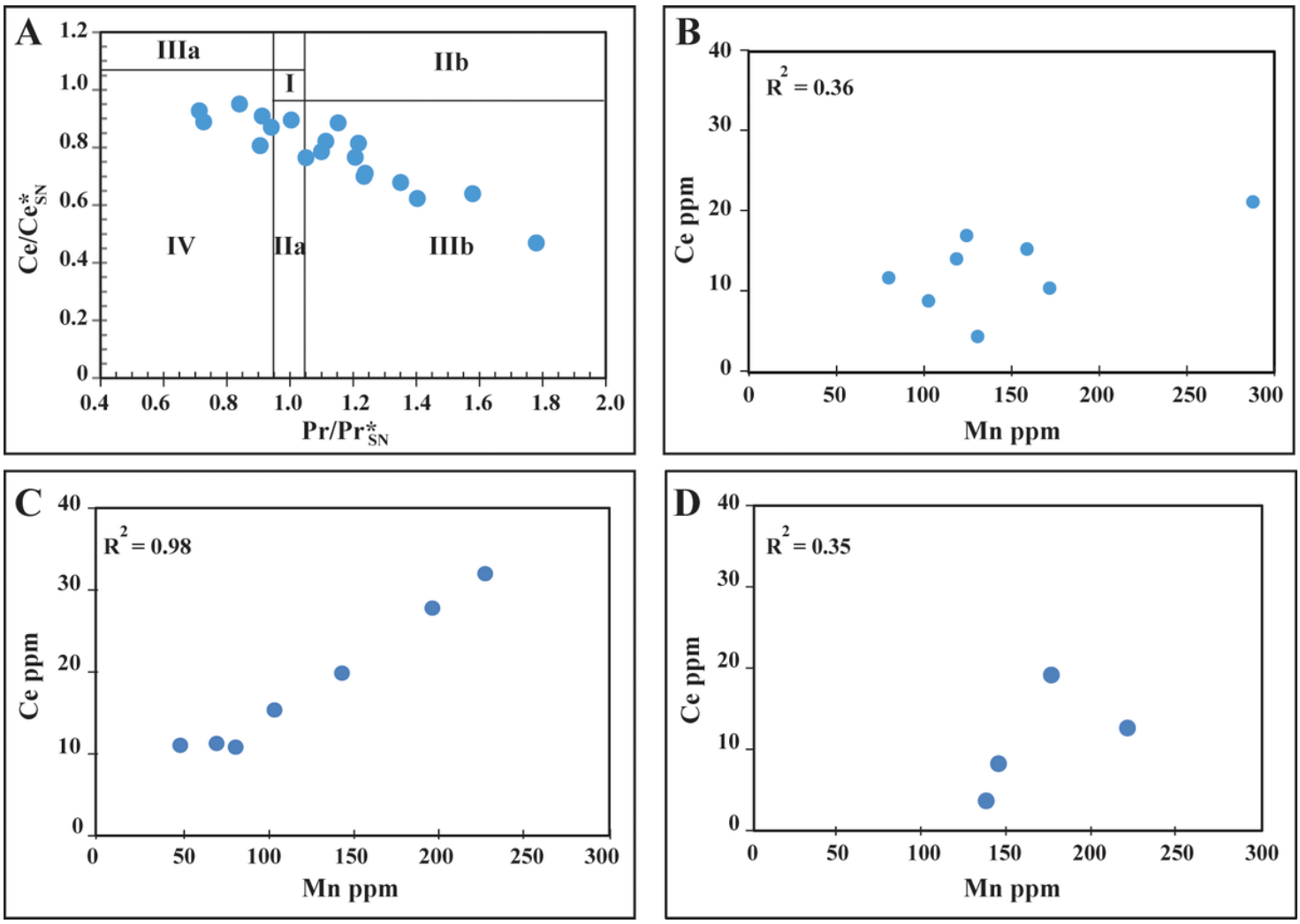

Figure 6

A) Samples on the Ce/Ce*- Pr/Pr* diagram fall in the IV, IIIb, and IIa fields. B-D) The correlation coefficients between Ce–Mn for depths of 0– 140 cm (B), 165–270 (C), and 290– 360 cm (D). The very high correlation coefficient between Ce- Mn in figure C highlights oxidizing conditions, but the low ones in figures B and D represent reducing conditions (Amin-Rasouli et al., 2021).

Figure 7

A- C. Photsshow secondary carbonate minerals in Karaftu Cave.

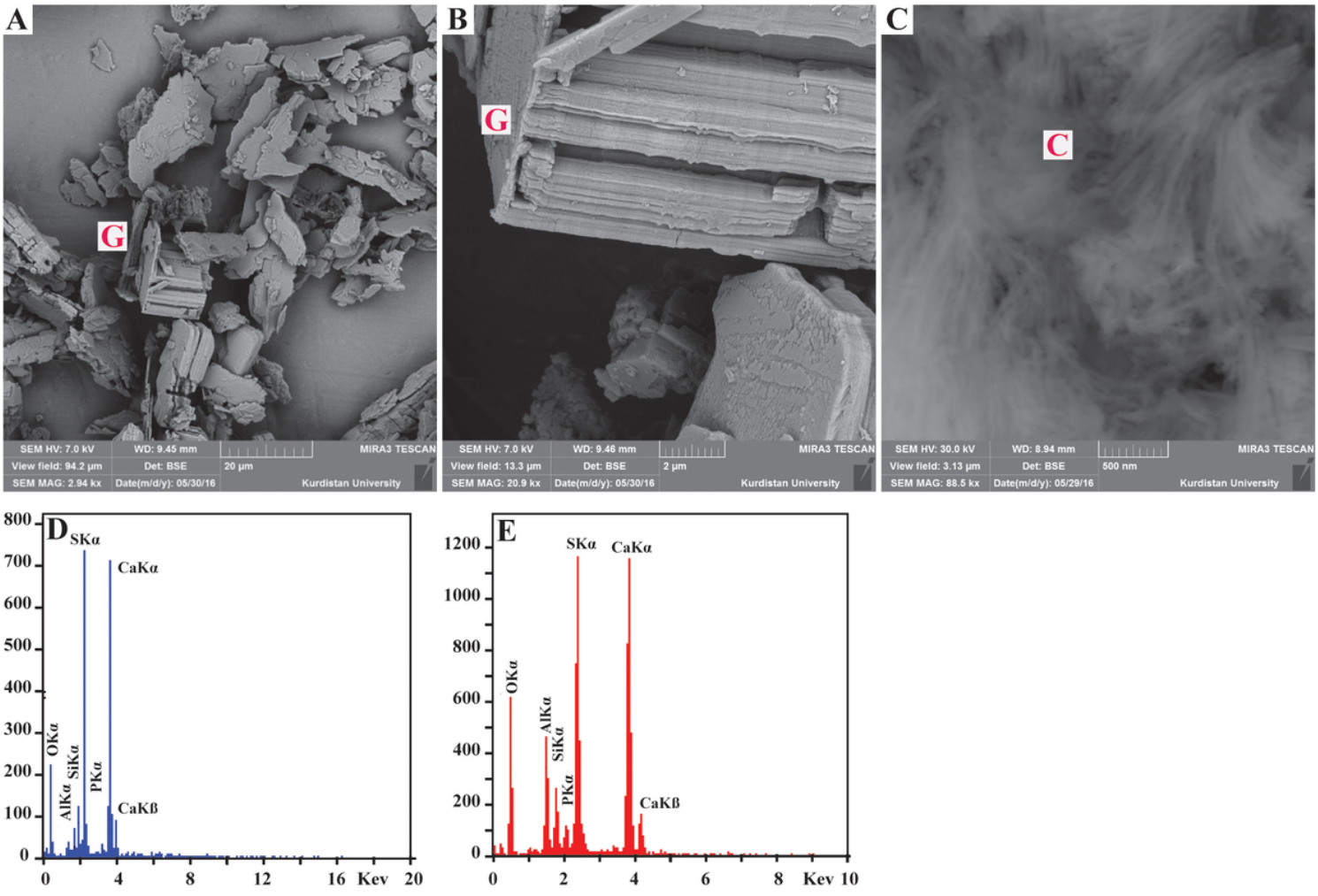

Figure 8

SEM images of identifying sulfate minerals in guano profile at Karaftu Cave: A, B) Gypsum, G. C) Cesanite ($Na_3Ca_2(SO_4)_3OH$), C. D, E) EDX spectra of gypsum (D) and cesanite (E) (Amin-Rasouli et al., 2022).

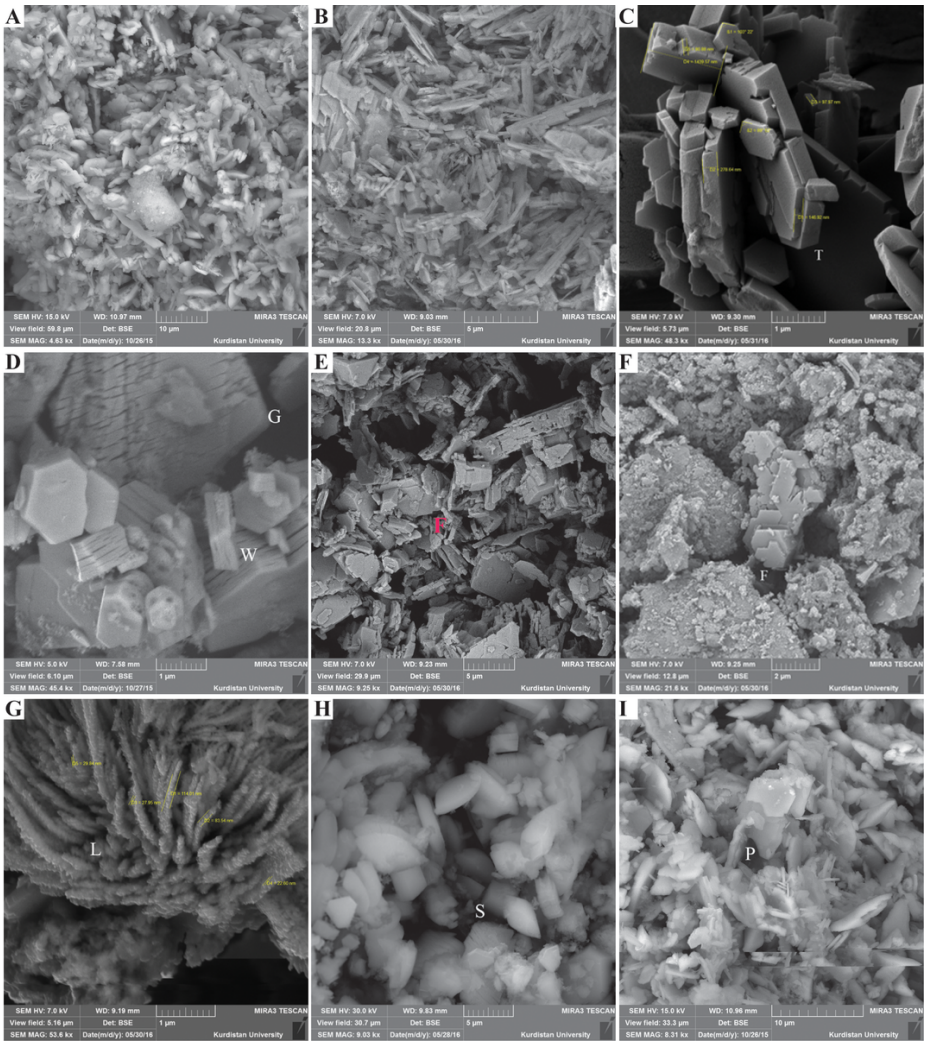

Figure 9

SEM images of phosphate minerals of guano deposits: A) Phosphammite ($(NH_4)_2HPO_4$). B) Brushite ($CaHPO_4.2H_2O$). C) Taranakite, T, $((K,Na)_3(Al,Fe^{3+})_5(PO_4)_2(HPO_4)_6.18H_2O$). D) Whitlockite, W, $(Ca_9(Mg,Fe)(PO_4)_6PO_3OH)$. E, F) Francoanellite, F $(H_6(K,Na)_3(Al,Fe^{3+})_5(PO_4)_8.13H_2O)$. G) Leucophosphite, L, $(KFe^{3+}{}_2(PO_4)_2OH.2H_2O)$. H) Spheniscidite, S, $((NH_4,K)(Fe^{3+},Al)_2(PO_4)_2OH.2H_2O)$. I) Pyrocoproite, P, $((Mg(K,Na))_2P_2O_7)$ (Amin-Rasouli et al., 2022).

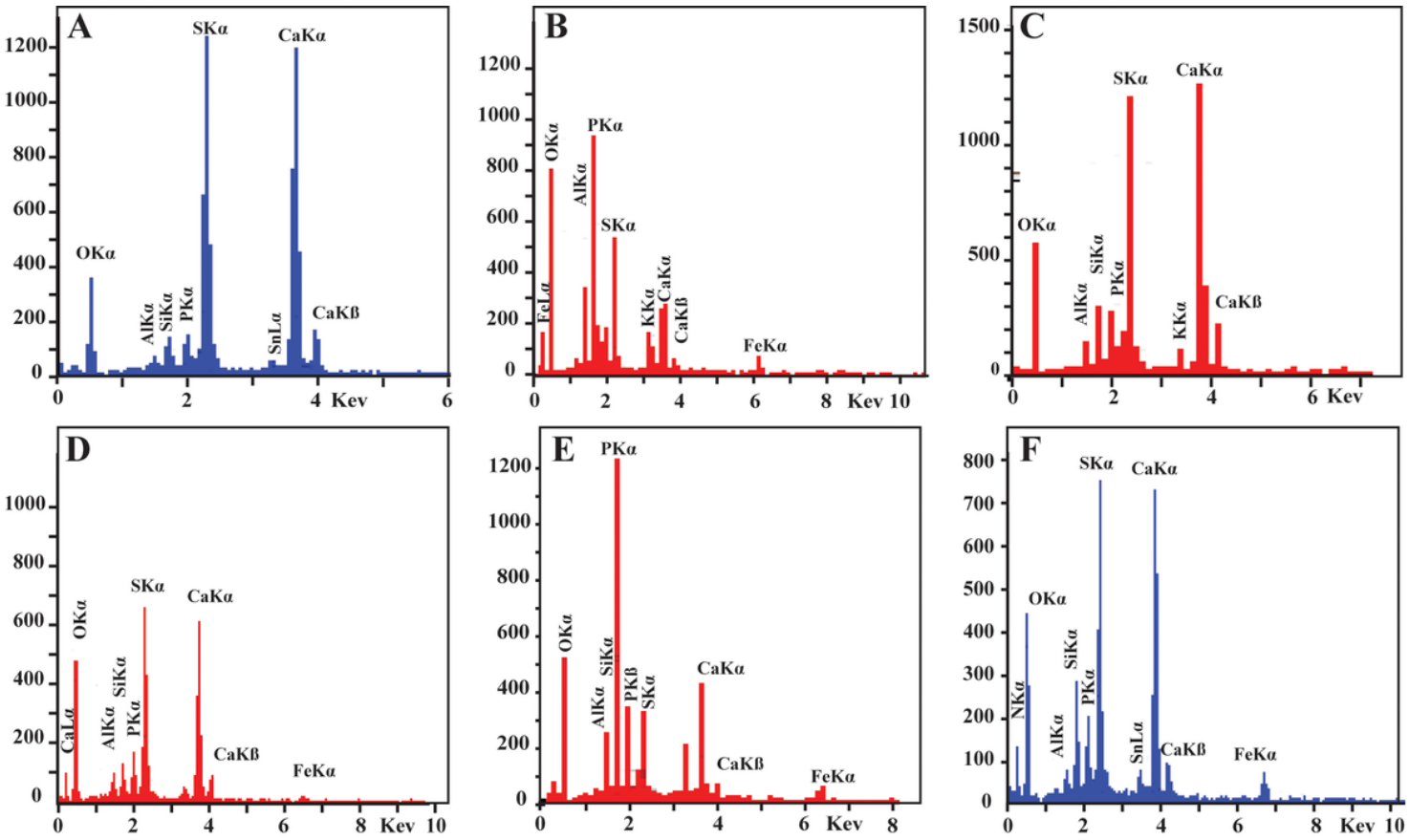

Figure 10

EDX spectra of phosphate minerals in the studied guano deposits. A) Phosphammite. B) Brushite. C) Taranakite. D) Whitlockite. E) Leucophosphite. F) Spheniscidite.

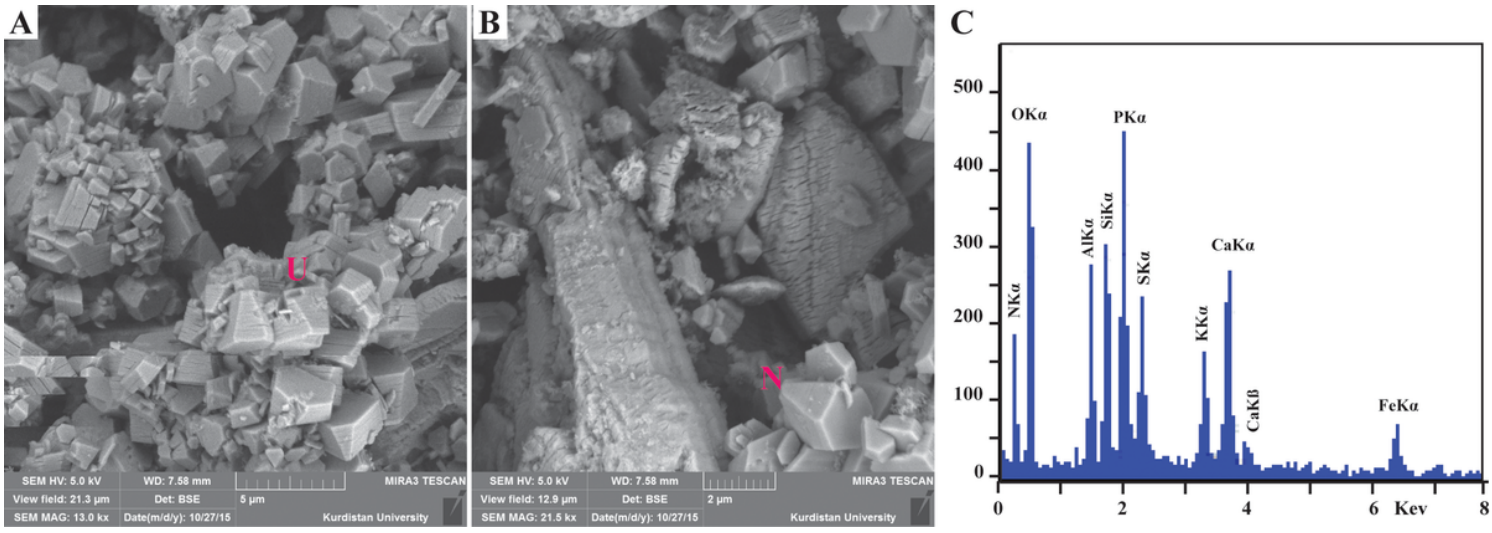

Figure 11

SEM images of nitrate minerals of guano deposits in the Karaftu Cave: A) Urea, U, ($CO(NH_2)_2$). B) Niter, N, (KNO3). C) Nitrogen element in EDX spectra (Amin-Rasouli et al., 2022).

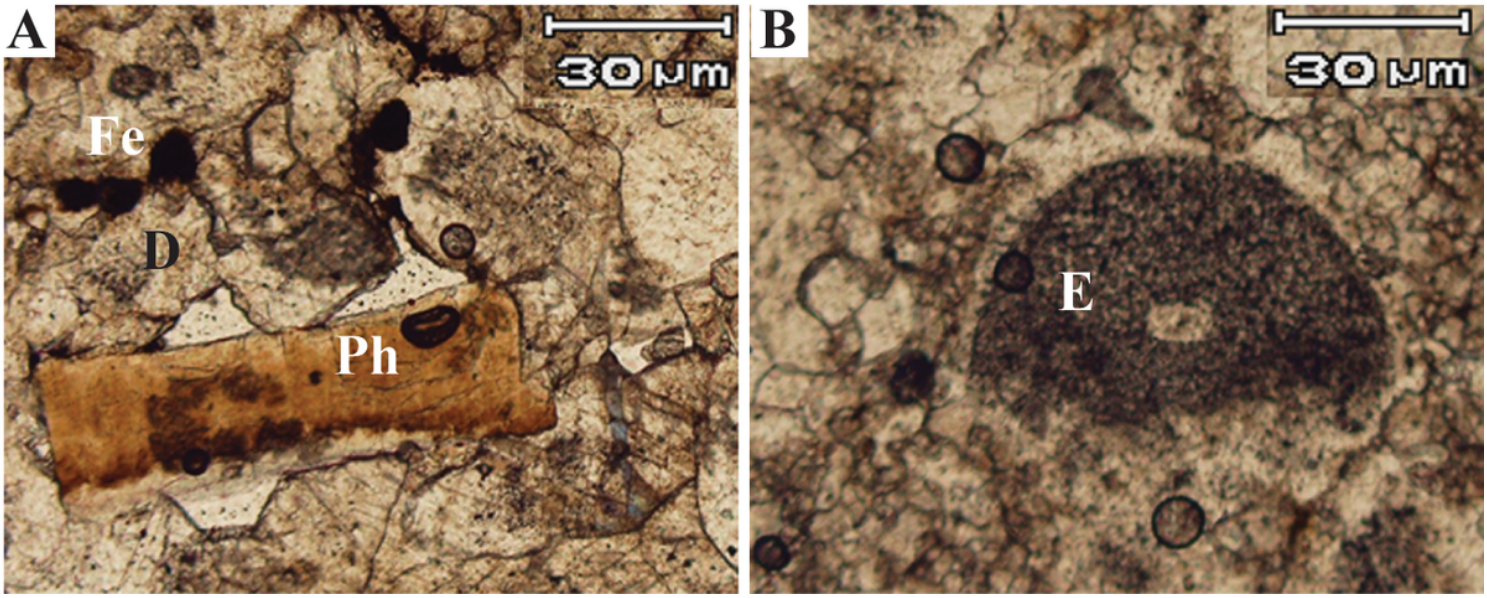

Figure 12

A) Fe- oxide (Fe), dolomite (D) minerals, and phosphatized particle (Ph) in the bedrock, ppl. B) Dolomitized echinoderm particle (E), ppl (Amin-Rasouli et al., 2022).

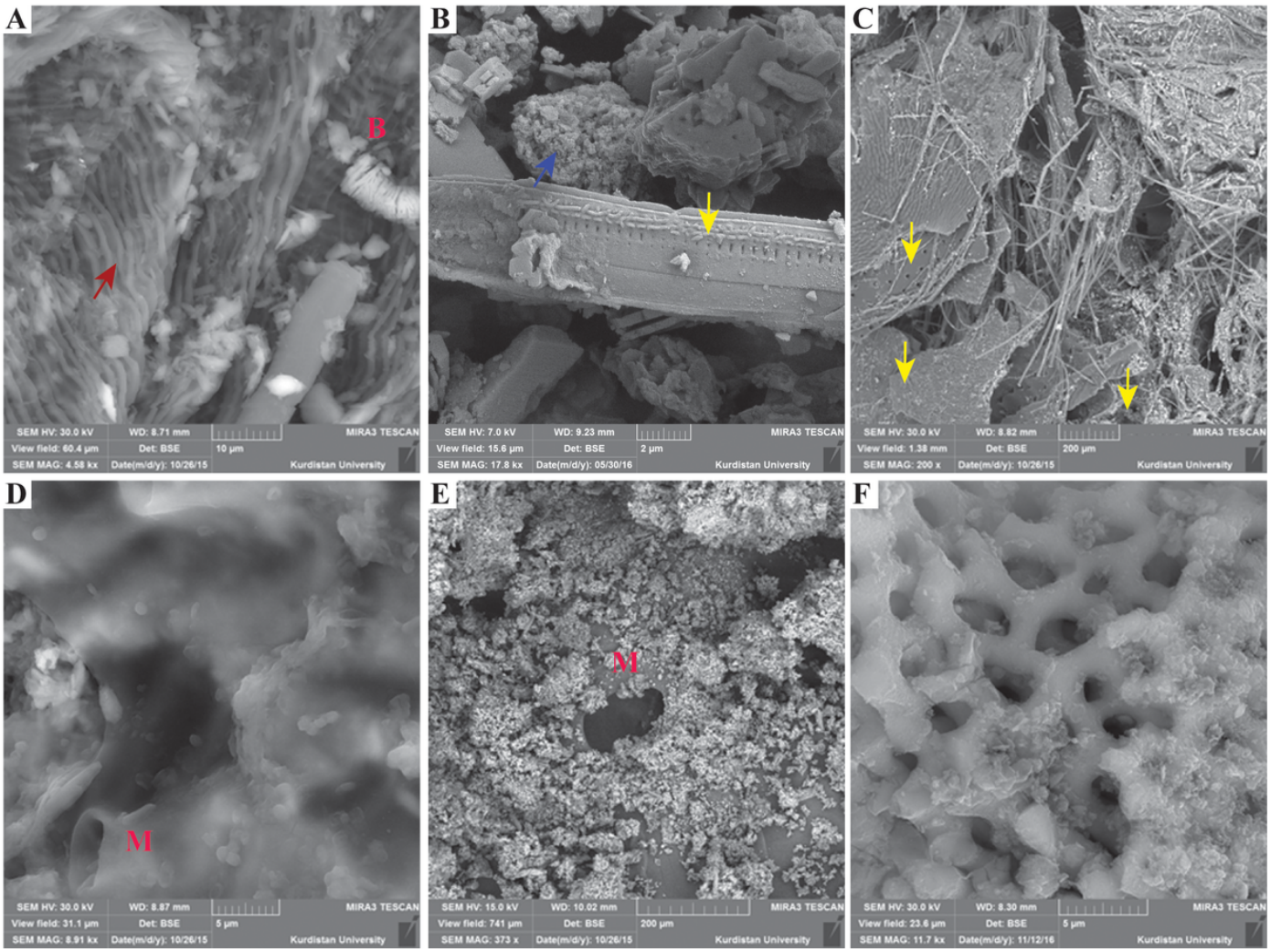

Figure 13

SEM images (A-C) from the top of the guano deposit showing: A) Cyanobacteria (red arrow) and Bacillus (B). B, C) Images show the deformation of guano components (purple arrow) due to exothermic reactions (B) and diatom remains (yellow arrows). D to F images from 165 cm depth: D, E) Microorganisms (M). F) Chitin particle (Amin-Rasouli et al., 2022).

Figure 14

A, B) Images show a pond on the guano deposits in Karaftu Cave. Note the difference between the depth of the pond in A (Photo taken in 2017) and B (Photo taken in 2022). C) The underground in the bat hall (Photo of the underground was taken from bat hall).